Resveratrol targets PD-L1 glycosylation and dimerization to enhance antitumor T-cell immunity

Sara Verdura[1,2,*], Elisabet Cuyàs[1,2,*], Eric Cortada[2,3,4], Joan Brunet[5,6,7,8], Eugeni Lopez-Bonet[9], Begoña Martin-Castillo[10], Joaquim Bosch-Barrera[2,5,6], José Antonio Encinar[11], Javier A. Menendez[1,2]

[1]Program against Cancer Therapeutic Resistance (ProCURE), Metabolism and Cancer Group, Catalan Institute of Oncology, Girona, Spain
[2]Girona Biomedical Research Institute (IDIBGI), Girona, Spain
[3]Cardiovascular Genetics Centre, Department of Medical Sciences, University of Girona, Girona, Spain
[4]Centro de Investigación Biomédica en Red de Enfermedades Cardiovasculares (CIBERCV), Madrid, Spain
[5]Medical Oncology, Catalan Institute of Oncology, Girona, Spain
[6]Department of Medical Sciences, Medical School University of Girona, Girona, Spain
[7]Hereditary Cancer Programme, Catalan Institute of Oncology (ICO), Bellvitge Institute for Biomedical Research (IDIBELL), L'Hospitalet del Llobregat, Barcelona, Spain
[8]Hereditary Cancer Programme, Catalan Institute of Oncology (ICO), Girona Biomedical Research Institute (IDIBGI), Girona, Spain
[9]Department of Anatomical Pathology, Dr. Josep Trueta Hospital of Girona, Girona, Spain
[10]Unit of Clinical Research, Catalan Institute of Oncology, Girona, Spain
[11]Institute of Research, Development and Innovation in Biotechnology of Elche (IDiBE) and Molecular and Cell Biology Institute (IBMC), Miguel Hernández University (UMH), Elche, Spain
*Equal contribution

Correspondence to: Javier A. Menendez, José Antonio Encinar; email: jmenendez@iconcologia.net, jmenendez@idibgi.org, jant.encinar@umh.es

ABSTRACT

New strategies to block the immune evasion activity of programmed death ligand-1 (PD-L1) are urgently needed. When exploring the PD-L1-targeted effects of mechanistically diverse metabolism-targeting drugs, exposure to the dietary polyphenol resveratrol (RSV) revealed its differential capacity to generate a distinct PD-L1 electrophoretic migration pattern. Using biochemical assays, computer-aided docking/molecular dynamics simulations, and fluorescence microscopy, we found that RSV can operate as a direct inhibitor of glyco-PD-L1-processing enzymes (α-glucosidase/α-mannosidase) that modulate *N*-linked glycan decoration of PD-L1, thereby promoting the endoplasmic reticulum retention of a mannose-rich, abnormally glycosylated form of PD-L1. RSV was also predicted to interact with the inner surface of PD-L1 involved in the interaction with PD-1, almost perfectly occupying the target space of the small compound BMS-202 that binds to and induces dimerization of PD-L1. The ability of RSV to directly target PD-L1 interferes with its stability and trafficking, ultimately impeding its targeting to the cancer cell plasma membrane. Impedance-based real-time cell analysis (xCELLigence) showed that cytotoxic T-lymphocyte activity was notably exacerbated when cancer cells were previously exposed to RSV. This unforeseen immunomodulating mechanism of RSV might illuminate new approaches to restore T-cell function by targeting the PD-1/PD-L1 immunologic checkpoint with natural polyphenols.

INTRODUCTION

Unlike immunologically "hot" tumors such as lung cancer, melanoma, and bladder cancer, most breast carcinomas are not inherently immunogenic. Consequently, they typically exhibit low T-cell infiltration and are unlikely to benefit from immune checkpoint-centric therapies [1–5]. Exceptions to this immunologically "cold" rule of breast carcinomas are the so-called basal-like [6–14] and HER2-positive [15–20] subtypes, both of which show evidence of immunogenicity including tumor immune infiltrates and stromal and intratumoral tumor-infiltrating lymphocytes, a good predictive marker for responses to immunotherapy. Correspondingly, the otherwise rare expression in most breast carcinomas of programmed death ligand-1 (PD-L1) – an archetypal immunosuppressive molecule on cancer cells that engages its receptor PD-1 on T-cells to suppress T-cell-mediated immune surveillance [21–23] – is markedly enriched in basal-like and HER2-positive tumors, thereby implying that PD-L1 confers a survival advantage in the tumor microenvironment (TME) of these specific breast cancer subtypes. However, the response rates reported in clinical trials for breast cancer with PD-1/PD-L1 checkpoint inhibitors as single agents have been rather disappointing (5–10%), although better clinical activities (up to 30%) and durable overall responses have been observed in patients with basal-like/HER2+ breast cancer and positive expression of PD-L1 [24–29]. Accordingly, the identification of new strategies to block the immune-inhibitory signal of PD-L1 in basal-like and HER2-positive subtypes is urgently needed.

In recent years, the cancer immunometabolism field has started to provide important insights into the pivotal role of metabolism in controlling immune cell function [30–35]. Indeed, much is now known about how the phenotypic switching of T-cells to be effective against tumor cells necessarily requires metabolic specialization, and how specific metabolic activities and tumor-driven shifts in the abundance of specific metabolites shape local immunosuppression and reduce the metabolic fitness of tumor-infiltrating lymphocytes. Indeed, the inhibitory nature of the metabolic interplay between tumor and immune cells in the TME supports its suitability as a target to overcome the immune escape of cancer cells and circumvent immunotherapy resistance. Accordingly, various combinations of immunotherapies with metabolic agents aimed to rewire T-cell fitness – by suppressing the immunosuppressive metabolic traits within the TME – are being tested in clinical trials [36–39]. Nonetheless, the appraisal of cancer cell-autonomous metabolic reprogramming as a *bona fide* driver of immune checkpoint signaling in tumor cells is a largely neglected area in cancer immunometabolism. Indeed, we are lacking even a minimal understanding of how pharmacological manipulations targeting core metabolic checkpoints such as AMPK, mTOR, and SIRT1, might fine-tune the expression of immune checkpoint receptors in cancer cells.

Here, we took advantage of the JIMT-1 cell line, a unique model of highly-aggressive basal-like/HER2-positive breast cancer naturally overexpressing the immunosuppressive molecule PD-L1 with 100% of the cells positive for PD-L1 [40], to explore the potential regulatory effects of mechanistically diverse metabolism-targeting drugs on PD-L1. By combining biochemical, computational, and microscopy approaches with label-free monitoring of T-cell activation, we provide the first evidence that the dietary polyphenol resveratrol (RSV) can directly target PD-L1 glycosylation and dimerization to enhance anti-tumor T-cell immunity.

RESULTS

Resveratrol increases the electrophoretic mobility of PD-L1 protein

PD-L1 is a type I transmembrane glycoprotein with an apparent molecular weight of ~45 kDa. We first examined the protein expression of PD-L1 in JIMT-1 cells cultured with the following metabolism-targeting drugs: the SIRT1 agonist RSV, the mitochondrial complex I inhibitor phenformin, the acetyl-coA carboxylase inhibitor soraphen A, the fatty acid synthase inhibitor C75, and the AMPK/mTOR regulators AICAR, compound C, PP242, and Torin (Figure 1A). Based on three independent experiments aimed to reflect the substantial variation of PD-L1 expression by multiple parameters including cell density, both phenformin and AICAR consistently downregulated the major PD-L1 form at ~45 kDa. By contrast, treatment with RSV increased the electrophoretic mobility of PD-L1, which led to the conspicuous appearance of an intense immunoreactive band with a slightly lower molecular size (Figure 1A).

Resveratrol disrupts N-linked glycosylation of PD-L1

Previous studies have unambiguously demonstrated that the ~45 kDa form of PD-L1 corresponds to the fully *N*-glycosylated mature protein [41–43]. As glycosylation of proteins often generates a heterogeneous migration pattern on immunoblots, such as that observed for PD-L1 in response to RSV treatment, we hypothesized that RSV might promote the accumulation of an aberrantly-glycosylated form of PD-L1. To test this, we re-evaluated the expression of PD-L1 in cells cultured with the antibiotic tunicamycin, which blocks *N*-linked

glycosylation by inhibiting the enzyme *N*-acetylglucosamine phosphotransferase, responsible for the initial steps in protein glycosylation (Figure 1B). A significant portion of the major ~45-kDa PD-L1 band was reduced to ~33 kDa upon tunicamycin treatment in control (RSV-untreated) cell cultures, which is known to represent the non-glycosylated form of PD-L1. The molecular weight shift to non-glycosylated PD-L1 was more evident in cells co-treated with RSV and tunicamycin, and the addition of tunicamycin also prevented the accumulation of the lower PD-L1 band that appeared in response to RSV as a single agent (Figure 1B). Also, in the presence of the protein synthesis inhibitor cycloheximide, the turnover of the RSV-induced smaller species of PD-L1 and of the non-glycosylated (~33 kDa) form of PD-L1 appeared to be faster than that of the fully-glycosylated (~45 kDa) form.
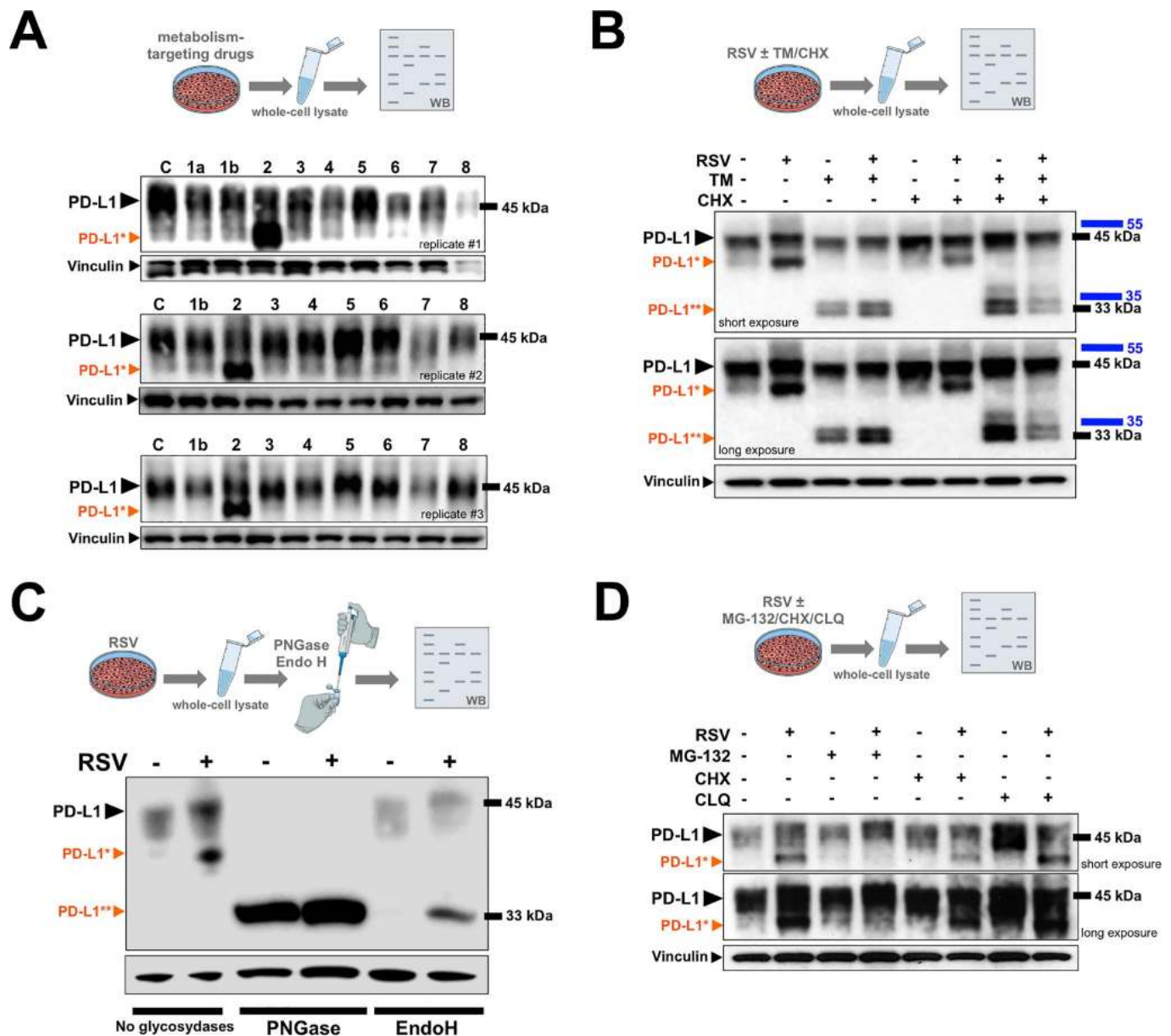
Figure 1. PD-L1 is abnormally glycosylated in response to resveratrol. (**A**) Representative immunoblot of PD-L1 protein in JIMT-1 cells cultured with or without metformin (1a), phenformin (1b), RSV (2), soraphen A (3), C75 (4), PP242 (5), Torin (6), AICAR (7), or compound C (8). (**B, D**) Representative immunoblots of PD-L1 protein in JIMT-1 cells cultured in the absence of presence of RSV, tunicamycin (TM), cycloheximide (CHX), chloroquine (CLQ), and/or MG-132. (**C**) PD-L1 glycosylation patterns obtained from cell lysates of RSV-treated or untreated control cells that were further treated with PNGase F and Endo H and analyzed by western blotting. (C: untreated control; black arrowhead, glycosylated PD-L1; *orange arrowhead, abnormal glycosylated PD-L1 form; **orange arrowhead, non-glycosylated PD-L1).

Whole cell lysates obtained from JIMT-1 cells cultured in the absence or presence of RSV were further incubated with either *N*-glycanase (PNGase F), which removes all types of *N*-linked (asparagine-linked) glycosylation (i.e., high mannose, hybrid, bi-, tri-, and tetra-antennary) or endoglycosidase H (Endo H), which removes only high mannose and some hydrid types of *N*-linked oligo-saccharides. Similar to the results with tunicamycin, PNGase F-driven removal of all *N*-linked glycan chains without regard to type completely blocked PD-L1 glycosylation irrespective of the absence or presence of RSV, as indicated by the conversion of the original pattern of PD-L1 post-translational glyco-modification to a discrete band corresponding to the non-glycosylated (~33 kDa) form (Figure 1C). By contrast, the addition of recombinant Endo H, which is known to cleave the high-mannose *N*-linked oligosaccharides found in the endoplasmic reticulum (ER), specifically prevented the aberrant glycosylated form of PD-L1 induced by the presence of RSV (Figure 1C).

Our results so far strongly suggest that the fraction of PD-L1 with a slightly lower molecular weight occurring in response to RSV is a non-fully, abnormally glycosylated form of PD-L1. Because PD-L1 protein stability is greatly influenced by its glycosylation state [41], we next determined the impact of the proteasome inhibitor MG-132 and the lysosomal inhibitor chloroquine on the RSV-induced faster migrating form of PD-L1. The abnormally glycosylated RSV-induced form of PD-L1 completely disappeared after treatment with MG-132 (Figure 1D), whereas chloroquine treatment notably protected the conspicuous PD-L1 migration pattern induced by RSV (Figure 1D).

Resveratrol directly targets N-linked glycan decoration of PD-L1

To substantiate that the RSV-induced aberrant glycosylated form of PD-L1 occurred concomitantly with the expected mode(s) of action of RSV, we first confirmed the well-known capacity of RSV to induce the endogenous expression of SIRT1 protein [42–44] (Figure 2A, left panels). Likewise, consistent with the ability of RSV to bind and inhibit histone HDAC enzymes [45, 46], RSV-treated JIMT-1 cells also showed increased p53 acetylation at lysine 382 [47]. The effects of RSV on PD-L1 glycosylation were neither prevented by the concurrent presence of the AMPK inhibitor compound C, nor by co-treatment with the SIRT1 inhibitor EX-527 [48] (Figure 2A, left panels). Moreover, the GSK3β inhibitors AR-18 (Figure 2A, middle panels) and LiCL (Figure 2A, right panels) failed to reverse the RSV-induced migration

pattern of PD-L1, thereby ruling out the possibility that RSV might indirectly disrupt N-linked glycosylation through GSK3β activation [49] (Figure 2A, right panels).

These findings are consistent with a direct (and SIRT1-, AMPK-, GSK3β-independent) effect of RSV on the PD-L1 *N*-linked glycosylation machinery (Figure 2B). Indeed, RSV treatment notably mimicked the ability of inhibitors blocking *N*-linked (but not O-linked) glycosylation (e.g., swainsonine, castanospermine, kifunensin, or 1-deoxy-mannojirimycin) to alter the migration pattern of glycosylated PD-L1 on SDS-PAGE [50]. Specifically, the capacity of RSV to operate as an antiglycation agent *via* direct inhibition of α-glucosidase I (GAA) [51–54] and/or α-mannosidase I (α-Man I) [55, 56] would suffice to explain the ability of RSV to generate an Endo H-sensitive, high-mannose *N*-linked glycan form of PD-L1 in the ER (Figure 2B). In an attempt to provide a computational explanation for the inhibitory activity of RSV against GAA, we performed molecular docking and molecular dynamics (MD) assays of RSV against high-resolution crystal structures of the yeast (4J5T [57]) and human (5NN4 [58]) forms of GAA. RSV was predicted to occupy the catalytic site of yeast GAA with a higher binding energy than that predicted for acarbose, a well-known competitive inhibitor of GAA [59–63] (Figure 3A–3C; supplementary information, Supplementary Figure S1 and Table S1). Conversely, several RSV clusters were predicted to interact with enzymatic pockets distant to the active site of human GAA (Figure 4, top panels), which was accurately predicted to be occupied by acarbose (Figure 4, bottom panels; Supplementary Table S2). When we extended the *in silico* studies to α-Man I (i.e., ER 1,2-α-mannosidase (5KIJ) [64]), the sole RSV cluster predicted to interact with α-Man was found to occupy the catalytic site of the enzyme and exhibited a binding energy even higher than that predicted for kifunensin, a well-known pharmacological inhibitor of α-Man I [65, 66] (Figure 5A; Supplementary Table S3). Although the generation of a homology model of α-Man II predicted the ability of numerous clusters of RSV to interact with several enzymatic pockets including the active site (Figure 5B), the energy binding was lower than that predicted for α-Man I. Considering both the trajectories and the solvation/binding free energy differences (supplementary information, Supplementary Figure S2) of the different RSV-enzyme complexes following MD simulations up to 100 ns, the computational behavior of RSV was compatible with that of a non-competitive inhibitor bound to allosteric sites in the case of human GAA and of a competitive inhibitor capable of stably occupying the catalytic site in the case of human α-Man I.

Resveratrol inhibits the cell membrane localization of glycosylated PD-L1

We next investigated whether the ability of RSV to target PD-L1 glycosylation altered PD-L1 membrane trafficking. Light microscopy observations suggested that RSV induced a hypertrophy-like phenotype in treated JIMT-1 and MDA-MB-231 cells (Figure 6, top panels), a second PD-L1-overexpressing breast cancer model representative of the basal-like subtype [40, 67, 68] as indicated by the transformation of spindle-shaped control cells to more enlarged, irregular, and flattened cell morphologies after switching to culture medium with RSV (Figure 6, top panels). Also, immuno-fluorescence microscopy using an antibody directed against an intracellular epitope of PD-L1 showed PD-L1 enrichment both in the plasma membrane and in specific cytoplasmic vesicular-like compartments (Figure 6, bottom panels). A more detailed analysis showed that cell membrane PD-L1 signals were clearly diminished in response to RSV, and this was accompanied by an increase in the number of mostly perinuclear aggresome-like, inclusion bodies.
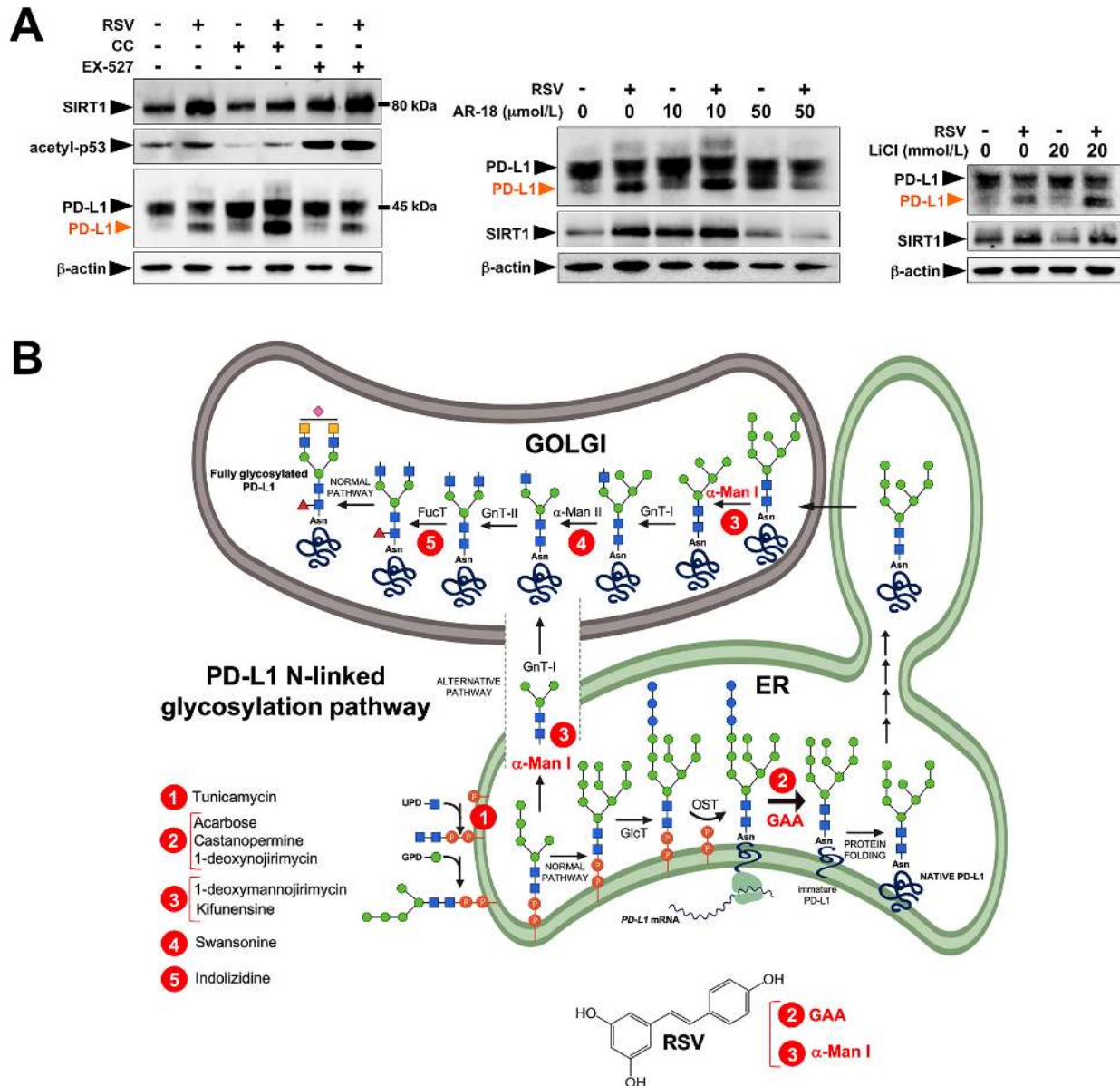

Figure 2. Resveratrol alters PD-L1 *N*-glycosylation in a SIRT1-, AMPK-, and GSK3β-independent manner. (**A**) Representative immunoblot of SIRT1, acetyl-p53 (Lys382), and PD-L1 in JIMT-1 cells cultured with or without RSV in the absence or presence of the AMPK inhibitor compound C, the SIRT1 inhibitor EX-527, and the GSK3β inhibitors AR-18 and LiCl. (**B**) Schematic representation of the biosynthesis and processing PD-1 *N*-linked glycosylation pathway, showing the sites of action of well-known glycoprotein-processing enzymes inhibitors. RSV is proposed to operate as a direct inhibitor of GAA and/or α-Man I enzymatic activities.

The RSV-driven cell membrane-to-cytoplasm redistribution of PD-L1 was more apparent when we used an antibody specifically directed to the extracellular domain of PD-L1, revealing an evident decrease in cell membrane-associated PD-L1 and the apparent retention of PD-L1 in perinuclear compartments with a punctate staining pattern (Figure 6, bottom panels).

**Resveratrol lowers the tumor cytotoxicity threshold to T-cells**

Finally, we questioned whether RSV-induced abnormal glycosylation of PD-L1 would increase the susceptibility of basal-like/HER2+ breast cancer cells to T-cell elimination. To do this, we used an impedance-based assay (xCELLigence system) for real-time and
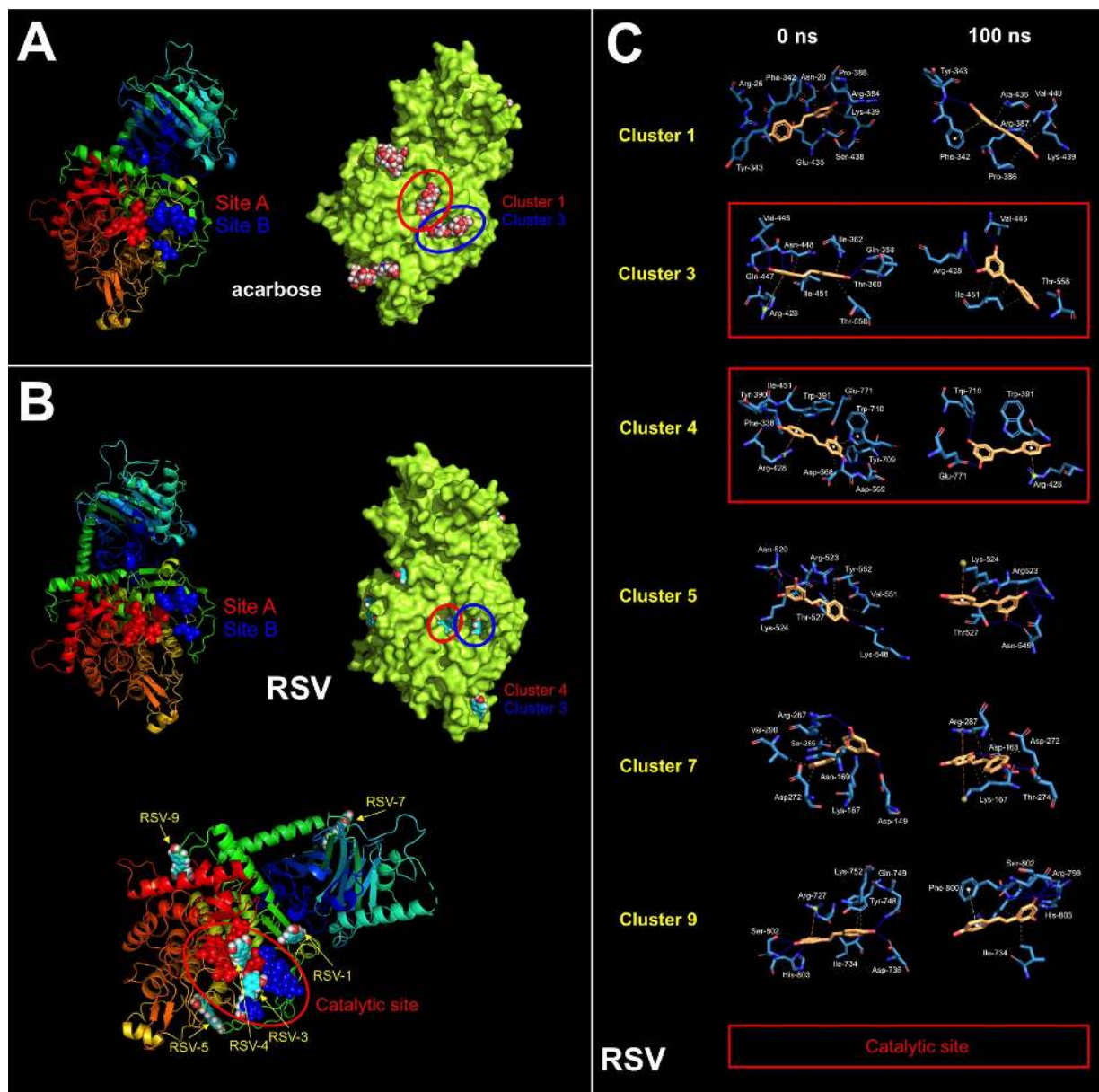
Figure 3. Resveratrol is predicted to bind the catalytic site of yeast GAA. Surface and backbone representations of yeast GAA showing the computationally predicted location of acarbose (**A**) and RSV (**B**) clusters. "Site A" refers to the pocket containing the proposed catalytic residues of yeast GAA whereas "site B" refers to a second cavity roughly 12 Å away from the active site pocket of yeast GAA [57]. (**C**) A detailed map of the molecular interactions of RSV in each cluster before (0 ns) and after 100 ns of molecular dynamics simulation. Each inset shows the detailed interactions of each RSV cluster docked to yeast GAA using the PLIP algorithm [124], indicating the participating amino acids involved in the interaction and the type of interaction (hydrogen bonds, hydrophilic interactions, salt bridges, Π-stacking, etc). Figures were prepared using PyMol 2.3 software.

label-free assessment of T-cell-mediated killing of PD-L1-expressing JIMT-1 cells [69, 71]. Briefly, impedance (or opposition) to an electric current occurs when adherent (tumor) cells bind to electrode plates; conversely, electrical impedance is reduced when tumor cells detach following killing, which can be measured by the real-time cell analyzer. The addition of T-cells in suspension over a monolayer of adherent tumor cells does not influence the impedance measurements as they do not contact with the electronic sensor; however, we could specifically detect

T-cell activation events as the induction of T-cell-mediated tumor cell death results in morphological and detachment events that can readily be detected *via* changes in impedance. At a T-cell-to-cancer cell ratio of 5:1, we observed cytolytic activities as low as 15–17% following the addition of T-cells to JIMT-1 cells (Figure 7). When JIMT-1 cells were pre-treated with RSV before exposure to T-cells, we observed a significantly more robust cytolytic activity that reached >50% of the tumor cell population (Figure 7).
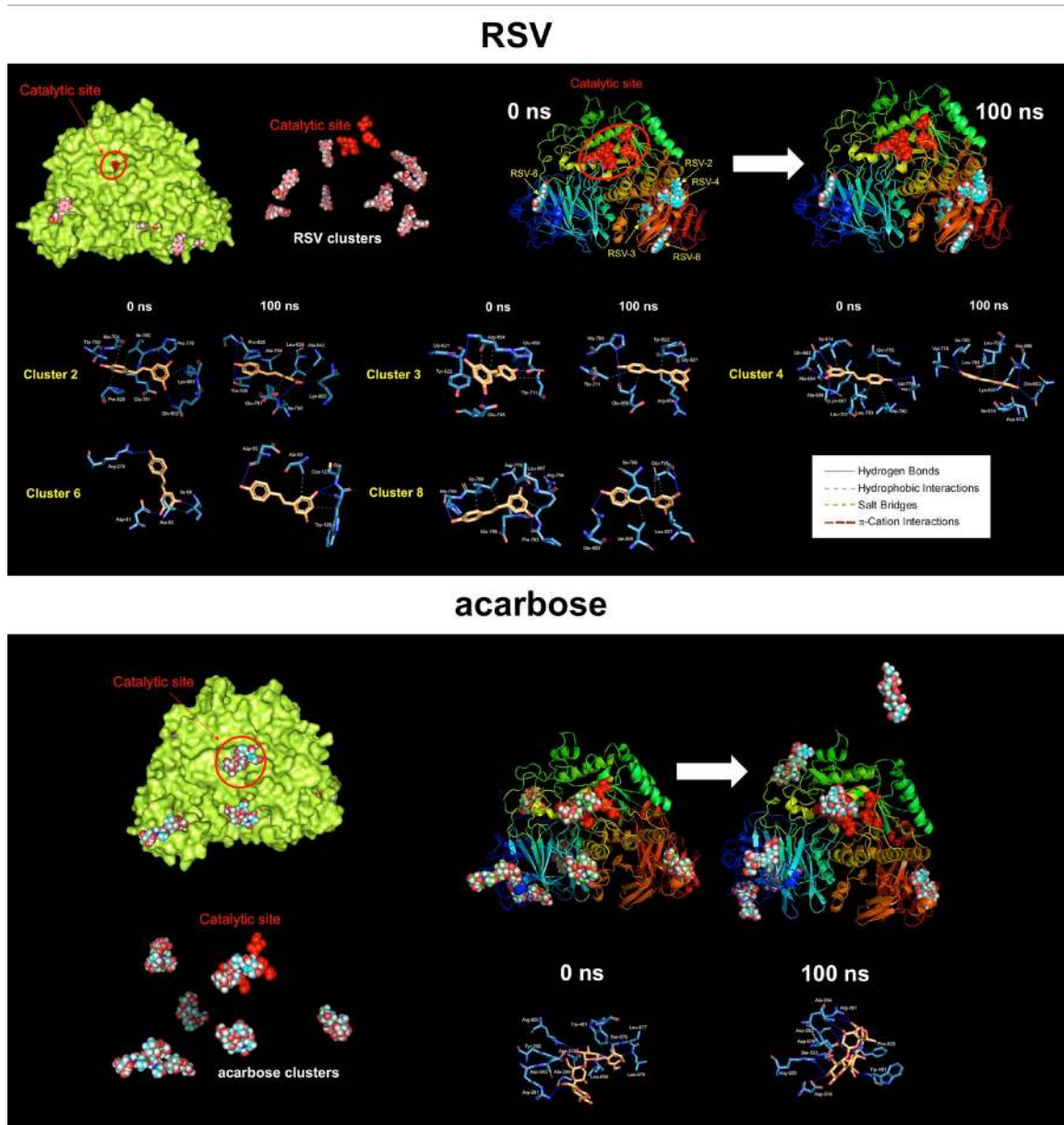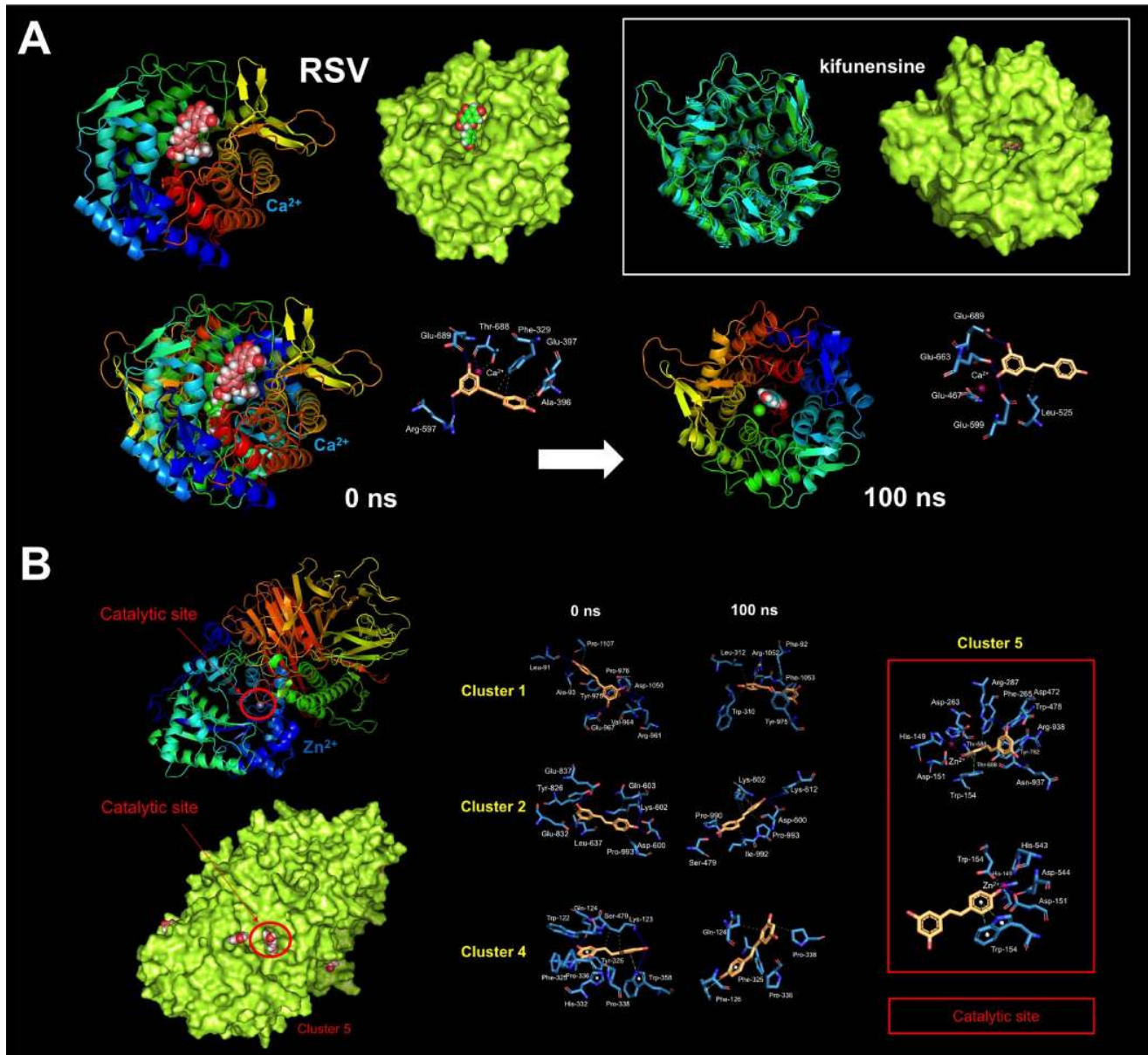

Figure 4. Resveratrol is predicted to bind allosteric sites in the surface of human GAA. Surface and backbone representations of human GAA showing the computationally-predicted location of RSV (top panels*)* and acarbose (bottom panels) clusters. A detailed map of the molecular interactions of RSV and acarbose in each cluster before (0 ns) and after 100 ns of molecular dynamics simulation. Each inset shows the detailed interactions of each RSV/acarbose cluster docked to human GAA using the PLIP algorithm [124], indicating the participating amino acids involved in the interaction and the type of interaction (hydrogen bonds, hydrophilic interactions, salt bridges, Π-stacking, etc). Figures were prepared using PyMol 2.3 software.

RSV is predicted to target PD-L1 dimerization

The strong exacerbation of the cytotoxic activity of T-cells against RSV-treated cancer cells raised the suspicion that additional PD-L1-targeted RSV mechanisms of action might be involved. We speculated that such non-mutually exclusive mechanisms might involve RSV binding to the dimerization surface of PD-

L1, which is the same employed by PD-L1 to interact with PD-L1 [71–77]. Computer-aided docking/MD simulations predicted the capacity of RSV to occupy the cavity formed by two PD-L1 monomers (ΔG=-9.252 kcal/mol) in a manner closely mimicking that of BMS-202 (ΔG=-11.11 kcal/mol), a small-molecule capable of inhibiting the PD-1/PD-L1 interaction by inducing PD-L1 dimerization through the PD-1 interacting surface


Figure 5. Resveratrol is predicted to bind the catalytic site of human α-mannosidases. Surface and backbone representations of human α-Man I (**A**) and homology model of human α-Man II (**B**) showing the computationally predicted location of RSV clusters. A detailed map of the molecular interactions of RSV in each cluster before (0 ns) and after 100 ns of molecular dynamics simulation. Each inset shows the detailed interactions of each RSV cluster docked to human GAA using the PLIP algorithm [124], indicating the participating amino acids involved in the interaction and the type of interaction (hydrogen bonds, hydrophilic interactions, salt bridges, Π-stacking, etc). The white inset in A shows a surface and backbone representations of human α-Man I docked to the α-Man I inhibitor kifunensine. Figures were prepared using PyMol 2.3 software.
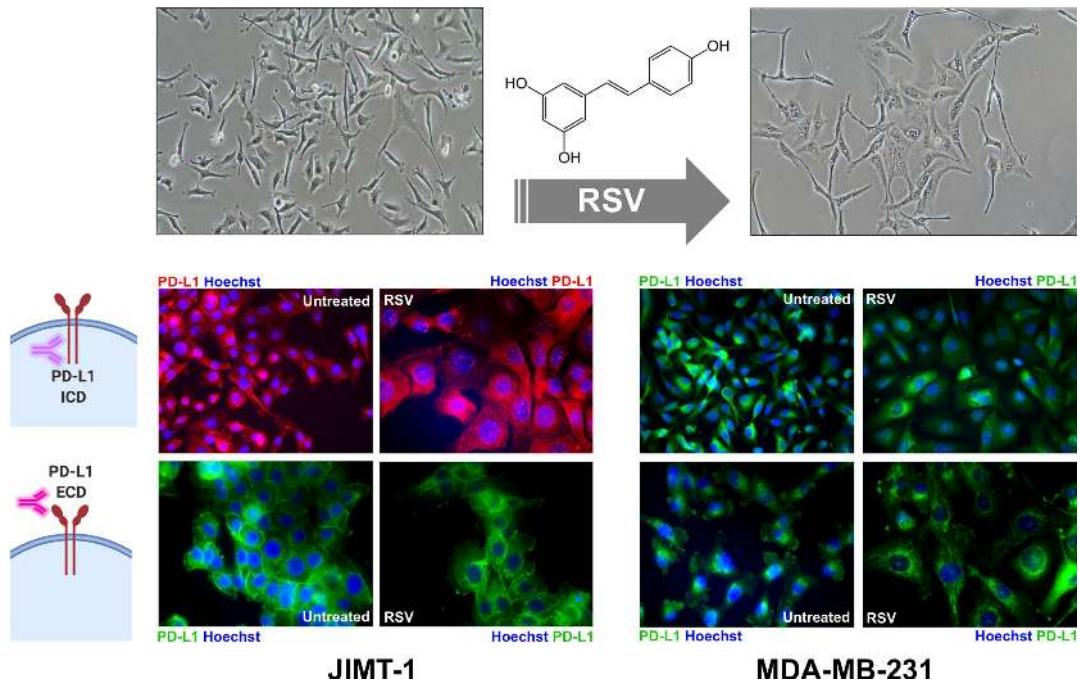
Figur*e* 6*. Resveratrol alters the sub-cellular expression pattern of PD-L1. Representative immunofluorescence staining of PD-L1 in JIMT-1 *(*left panels) and MDA-MB-231 (right panels) breast cancer cells cultured in the absence or presence of RSV, using an antibody directed against either an intracellular epitope (top panels) or an extracellular domain epitope (bottom panels) of PD-L1.
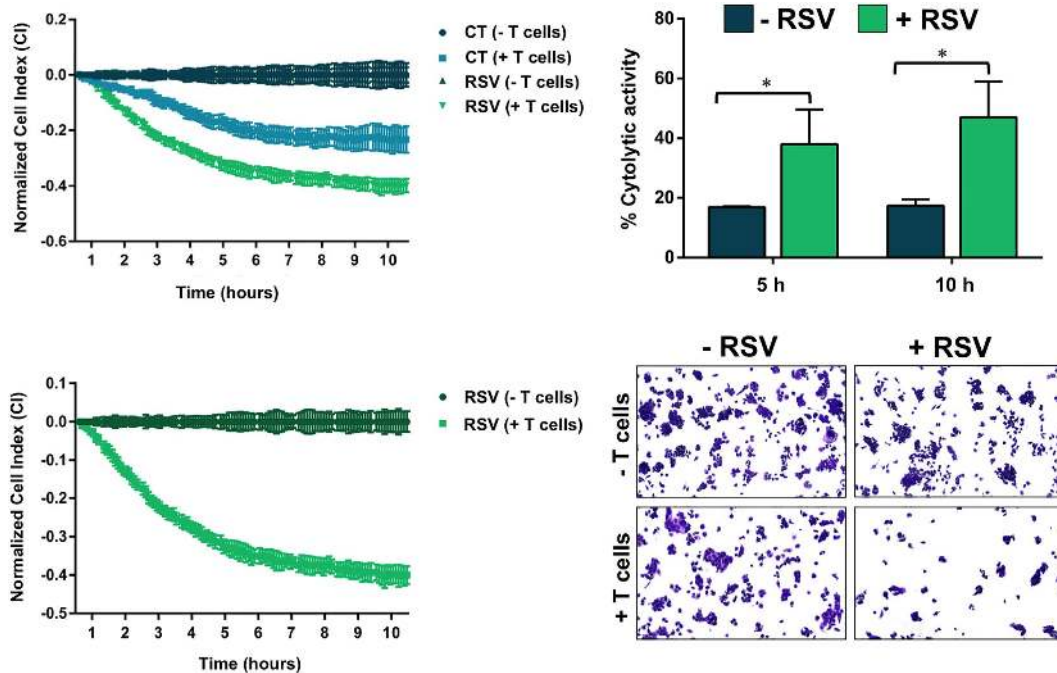
Figure 7. Resveratrol enhances the susceptibility to T-cell-mediated tumor cell killing. T-cell-mediated cell death of JIMT-1 cells pre-cultured in the absence of presence of RSV was measured using the xCELLigence system. Shown are the mean (±SD, n=3) of % lysis values calculated from the impedance-based lysis assay at 5 and 10 hours following the addition of T-cells. Also shown are microphotographs of representative T-cell-mediated cancer cell killing assays in which tumor cells were subjected to crystal violet staining. Statistical analysis was performed using GraphPad Prism 7, using two-way ANOVA with Sidak's multiple comparison post-test, comparing untreated *versus* RSV-treated per time (* = *P* < 0.01).

[71, 75] (Figure 8, *top*). The interacting mode of RSV with the dimeric PD-L1 complex included the key contribution of Ile54, Tyr56, Met115, Ala121, and Tyr123 residues on both monomers. An analysis of the RSV trajectory docked to the PD-L1 dimerization interface during a 100 ns period revealed a less than 5Å displacement compared with its initial position at the PD-L1 interaction interface (Figure 8, *bottom*). These findings, together with solvation binding energies as

high as 45 kcal/mol, provided computational insight into the putative capacity of RSV to target PD-L1 dimerization and block the PD-1/PD-L1 interaction. When we examined monomeric and dimeric conformations of PD-L1 by native gel electrophoresis, the presence of appreciable amounts of PD-L1 dimer was apparent in RSV-treated cells whereas the monomeric form of PD-L1 was the major species in untreated control cells (Figure 8, *bottom*).
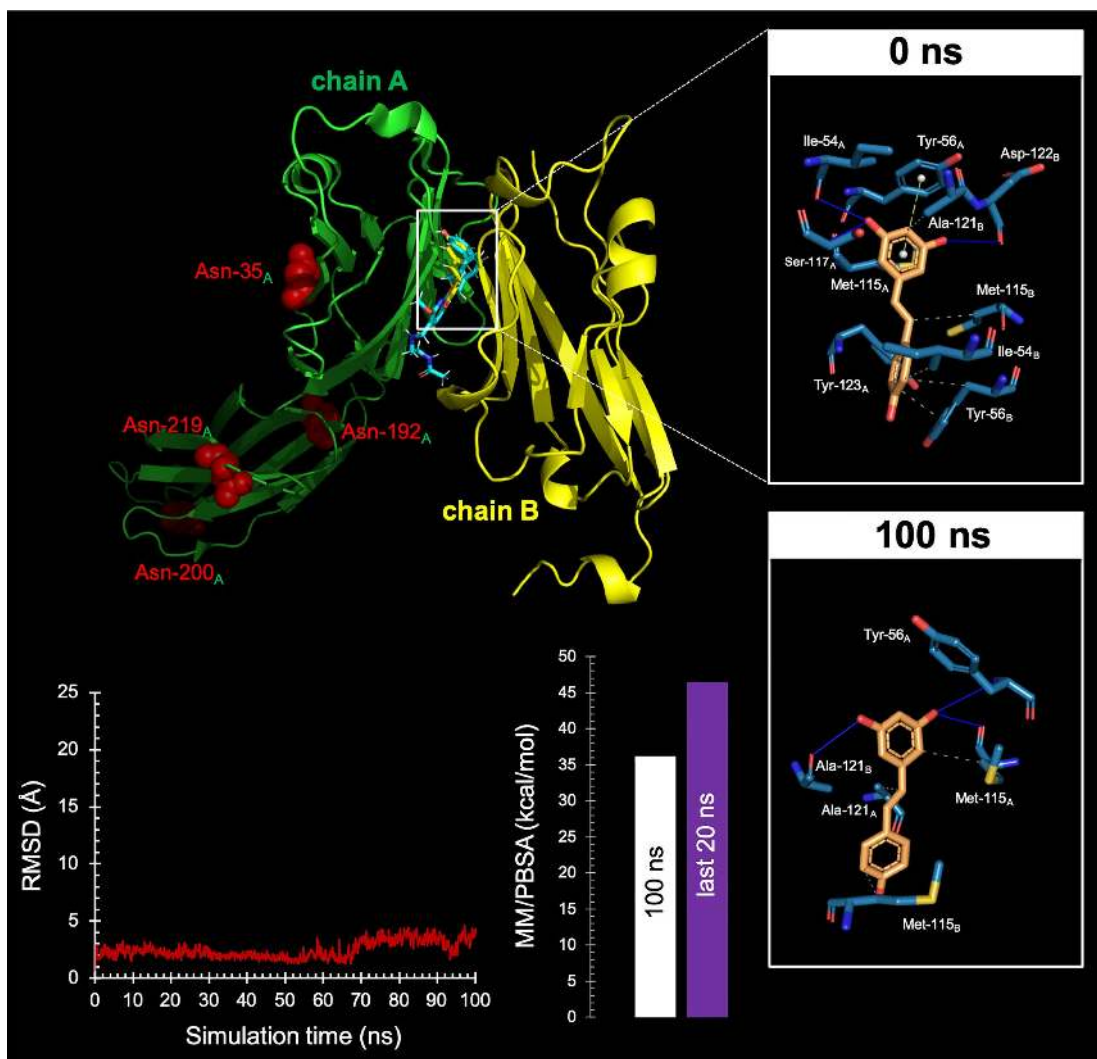

Figure 8. Resveratrol is predicted to bind the PD-1 dimer interface. *Top* Backbone representation of the PD-L1:PD-L1 dimer showing the computationally-predicted location of RSV (yellow) and BMS-202 (cyan). Chain A shows the location of the four Asn residues that can be glycosylated. The insets show the detailed maps of the molecular interactions of RSV with the amino acids at the hydrophobic pocket accommodating the BMS-202 inhibitor and formed at the PD-L1 dimer surface before (0 ns) and after 100 ns of molecular dynamics (MD) simulation, indicating the participating amino acids involved in the interaction and the type of interaction (hydrogen bonds, hydrophilic interactions, salt bridges, Π-stacking, etc). *Bottom. Left.* Trajectory of the RSV-forming complex with the PD-L1 dimer. *Right.* Molecular Mechanics/Poisson-Boltzmann Surface Area free energy analysis of the PD-L1 dimer forming a complex with RSV using YASARA dynamics v19.9.17 software. The best-docked complex as the initial conformation for MD simulation followed by 1000 snapshots (100 ns) obtained from the MD trajectory were employed to calculate the values of free energy binding of RSV. Additionally, the average value calculated for the last 200 snapshots (20 ns) is also displayed. YASARA-calculated binding energy provides positive values when the predicted binding is strong and stable whereas negative values indicate no binding. Figures were prepared using PyMol 2.3 software.

DISCUSSION

We provide the first demonstration that RSV targets the immune evasion capacities of cancer cells by directly disrupting *N*-glycan branching and promoting dimerization of PD-L1, thereby impeding the correct localization of PD-L1 to the plasma membrane, preventing the PD-1 interaction surface of PD-L1 and, consequently, increasing the susceptibility of bio-logically aggressive cancer cells to T-cell-mediated cell death (Figure 9).

The recently discovered ability of the mitochondrial I inhibitor metformin to target PD-L1 in cancer cells [67] provides support to the notion that the cancer cell-auto-nomous metabolic status can shape the composition of immune checkpoints in cancer cells. The activated form of AMPK generated in response to the metabolic crisis induced by metformin has been found to directly phosphorylate PD-L1 in a manner that promotes its abnormal glycosylation, resulting in ER accumulation and ER-associated protein degradation [39, 67]. We here characterized the unforeseen ability of RSV to disrupt *N*-linked glycosylation of PD-L1 and consequently reduce PD-L1 maturation and, ultimately, hamper its cancer cell surface-associated expression. Unlike metformin, however, the ability of RSV to generate a high mannose, abnormally glycosylated form of PD-L1 does not rely on its SIRT1-activating activity and also appears not to involve the well-known capacity of RSV to activate a
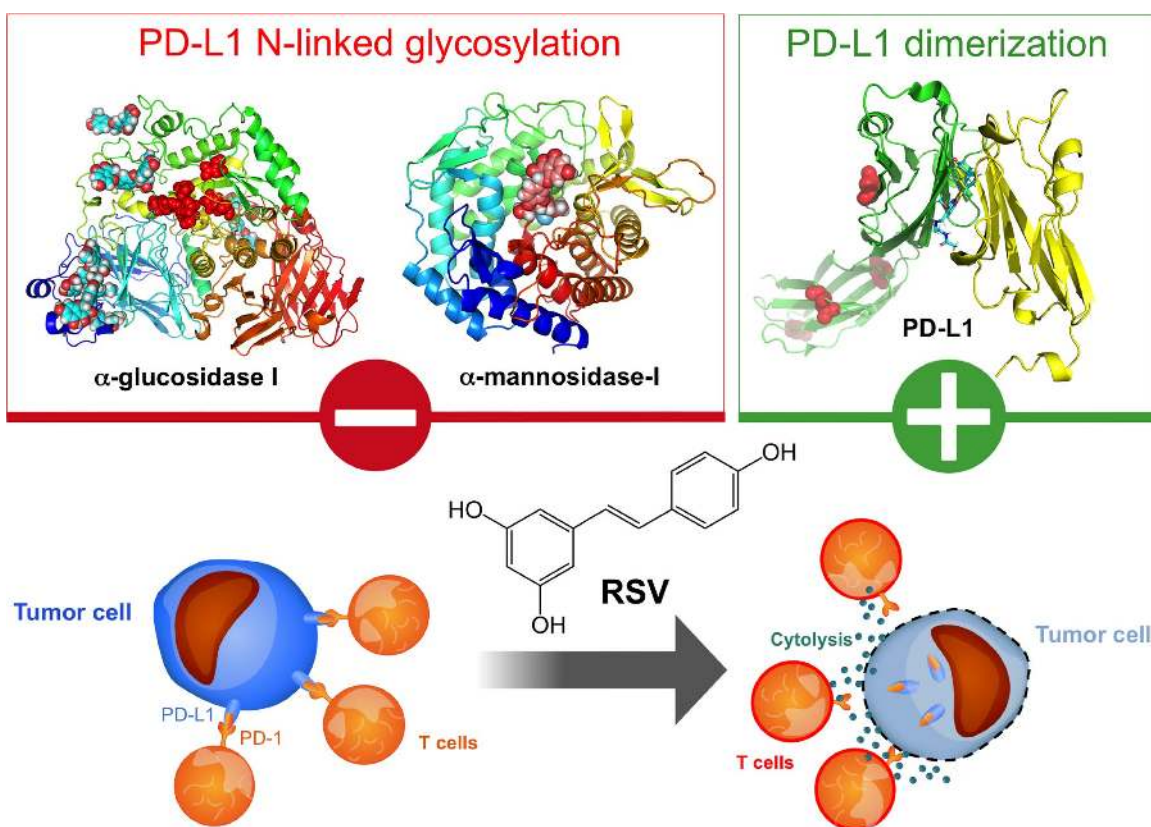
Figure 9. Resveratrol enhances antitumor T cell immunity by promoting abnormal glycosylation and dimerization of PD-L1. Post-translational modifications such as glycosylation, phosphorylation, palmitoylation or ubiquitination are essential for the folding, intracellular transport, and stabilization of the PD-L1 protein [41, 110–114]. PD-L1 is highly glycosylated, and *N*-linked glycosylation of PD-L1 critically maintains its protein stability and is required for its interaction with PD-1 to efficiently suppress T-cell activity. Recently, Bristol-Myers Squibb (BMS)-developed compounds with a common (2-methyl-4-biphenylyl)methanol scaffold have been reported to block the PD-1/PD-L1 interaction by interacting with the cavity formed by the two PD-L1 monomers and inducing the dimerization of PD-L1 [71–77]. Structural studies have revealed a dimeric protein complex with a single small molecule that stabilizes the dimer and thereby occludes the PD-1 interaction surface of PD-L1. We propose that RSV is a naturally occurring, double-strike PD-1/PD-L1 immune checkpoint inhibitor capable of directly blocking the enzymatic machinery in charge of the *N*-linked glycosylation of the nascent PD-L1 at the endoplasmic reticulum or directly binding to PD-L1 surfaces to induce PD-L1 dimerization and block PD-1 binding. This unforeseen ability of RSV to directly interfere with PD-L1 stability and trafficking impedes the correct targeting of PD-L1 to the cancer cell plasma membrane and ultimately elicits drastically enhanced cytotoxic T-lymphocyte immune-surveillance against tumor cells. These findings might illuminate new approaches to restore T-cell function by targeting the PD-1/PD-L1 immunologic checkpoint with natural polyphenols.

positive feedback between AMPK and SIRT1 [78–80]. Rather, RSV likely operates as a direct inhibitor of glycoprotein-processing enzymes such as GAA and α-Man I (Figure 6), which trim terminal glucoses and mannose from nascent PD-L1, a crucial process for proper PD-L1 protein folding [81, 82]. The finding that the occurrence of the Endo H-sensitive abnormal glycosylated form of PD-L1 induced by RSV was diminished by the protein synthesis inhibitor cycloheximide, completely cleared by the proteasome inhibitor MG-132, and notably protected by the autophagy inhibitor chloroquine, altogether support a mechanism of action in which: 1) RSV might directly hinder GAA/α-Man I-driven trimming of glucoses and mannose immediately after the lipid-linked oligosaccharide precursor is transferred to Asn residues of nascent PD-L1 protein. Such a direct blockade of key glycoprotein-processing enzymes prevents the PD-L1 glycoprotein from attaining its native conformation because GAA and α-Man I ensure that, after correct folding, the processed (high-mannose) PD-L1 glycoprotein can move to the Golgi where N-linked glycans can be further remodeled; 2) The consequent imbalance between the amount of unfolded/misfolded PD-L1 protein in the ER lumen and the capacity of the ER machinery to refold the population of aberrantly glycosylated PD-L1 should result in ER stress via the integrated networks of aggresome, proteasome, and autophagy. Future studies are warranted to clarify whether, upon proteasome inhibition, the RSV-induced non-fully glycosylated (unstable) PD-L1 form might become polyubiquitinated [41] and undergo selective degradation via the autophagy-lysosomal pathway; and 3). Lastly, the glycosylation-targeted regulatory mechanism of RSV prevents the complete translocation of the fully-glycosylated population of PD-L1 to the cell membrane and, because the interaction between PD-L1 and PD-1 is modulated specifically by N-linked glycosylation [50], abrogates the binding of PD-1 to PD-L1, thereby providing a mechanism to switch on T-cell activity. Accordingly, impedance-based real-time analysis showed that cytotoxic T-lymphocyte activity was dramatically augmented when PD-L1-over-expressing JIMT-1 cancer cells were previously exposed to RSV.

Our findings might provide a foundation to exploit the N-glycan biosynthesis-targeted inhibitory activity of RSV as a new strategy to safely alter PD-L1 glycosylation in vivo. Although targeting the surface distribution of PD-L1 by modulating N-glycan branching is emerging as an exciting approach to boost the immune system against cancer cells [50, 83–85], the clinical development of currently existing inhibitors that impact processing or "trimming" of the glucosylated, high-mannose side chains by inhibiting one or more of the specific processing glycosidases/mannosidases, is still lacking regarding effective modifications capable of improving their therapeutic efficacy, selectivity, potency, and tolerability. Acknowledging the poor bioavailability (<1%) of orally-administered RSV [86, 87], the capacity of RSV-like strategies to target N-glycan branching of PD-L1 and, consequently, decrease the T-cell cyto-toxicity threshold via targeting of glycoprotein-processing enzymes such as GAA and α-Man I might be a potential treatment option for cancer patients exhibiting a high neo-antigen, immunologically-active phenotype capable of attracting immune cells that ultimately triggers an unsuccessful tumor-immune cell interaction via PD-L1/PD-1 engagement [24–29, 88–90]. Early studies by Lucas et al. [91] showed that various colorectal and breast cancer cells (e.g., low PD-L1-expressing BT-474 and SK-Br3 cell lines) exposed to high concentrations of RSV upregulated PD-L1. The authors claimed that a potential upregulation of PD-L1 in vivo by RSV would render tumor cells more sensitive to immune checkpoints targeting PD-L1 [91], a counterintuitive hypothesis in terms of the potential chemopreventive value of RSV when considering that a putative upregulation of PD-L1 by RSV could enable pre-cancerous lesions to avoid antitumor immunity. Chin et al. [92] reported that the ability of the thyroid hormone L-thyroxin (T_4) to inhibit the anti-cancer effects of RSV involves the up-regulation of PD-L1; conversely, RSV was found to down-regulate *PD-L1* expression. A complex interplay thus exists between RSV and PD-L1 that might present mutually antagonistic effects and might differentially occur in settings where baseline PD-L1 is low or high [92, 93]. Baseline PD-L1 expression differs according to the molecular phenotype of breast carcinomas, with the highest expression occurring in those with basal-like traits and the lowest expression in those with luminal traits [40, 43, 44]. Each breast cancer subentity responds differentially to extrinsic and intrinsic factors, and a significant heterogeneity in PD-L1 expression can be observed even within PD-L1-overexpressing breast cancer populations. Thus, whereas PD-L1 upregulation might represent a protective mechanism against RSV in low PD-L1-expressing cancer cells, constitutive PD-L1 ovexpressors could possess an inherent susceptibility to glycosylation defects under ER stress conditions imposed by GAA/α-Man-I inhibitors such as RSV. Accordingly, inhibition of N-linked glycosylation by RSV has been shown to trigger ER-mediated apoptosis in ovarian cancer cells [49]. Perhaps more importantly, RSV has been recently shown to induce immunogenic cell death and immune activation in terms of increased cytotoxic T-cells, and to potentiate the therapeutic outcomes of a PD-1 antibody in murine and human models of ovarian cancer [94]. These immunomodulatory actions of RSV in the tumor microenvironment, together with its ability to interfere with the glycosylation-driven stability of the

immune checkpoint PD-L1, provides experimental evidence in support of combining RSV, which is virtually nontoxic with respect to its systemic effects, with immune checkpoint inhibitors, and might form the basis of future clinical trials.

Based on its mode of action involving core machineries (SIRT1 and AMPK) causally involved in the hallmarks of aging, such as epigenetic alterations, deregulated nutrient sensing, or mitochondrial dysfunction [62, 95], RSV has classically been considered an archetype member of the downstream type of calorie restriction mimetics (CRMs) including rapamycin, metformin, and polyamines (spermidine). Intriguingly, because normal human aging is characterized by a progressive decline in immune surveillance that is accompanied by PD-L1 upregulation to favor cancer initiation and progression even in the absence of a more complex mutational landscape [96–100], the suppression of PD-L1 signaling *via* direct targeting of PD-L1 glycosylation enzymes could represent a new immunometabolic mechanism through which RSV might prevent immune dysfunction and cancer development in the context of aging. Although there are conflicting data about whether the SIRT1 agonist activity of RSV might alleviate glucose intolerance in humans, it is reasonable to suggest that the ability of RSV to mimic acarbose in enhancing anti-cancer T-cell immunity [101, 102] uncovers an immunologic dimension to the previously observed capacity of RSV to exert anti-diabetic effects *via* direct inhibition of GAA [51–54, 103–105]. Acarbose, a pseudo-tetrasaccharide used to manage type 2 diabetes and a candidate drug in clinical trials targeting human aging based on its ability to improve health and lifespan in animal models [60–63, 106], is a potent competitive inhibitor of mammalian GAA, but is less effective against yeast GAA [51, 107]. RSV, however, has been shown to exert strong inhibition against both yeast and mammalian GAA activities [51, 53]. Although these discrepancies might be attributed to structural differences of the yeast and mammalian forms of the enzymes, we lack mechanistic insights capable of explaining the inhibition of GAA by RSV even at very low, clinically-relevant doses. In our hands, it was noteworthy that whereas RSV was *in silico* predicted to occupy the catalytic binding site of the yeast form of GAA with a higher binding energy than that predicted for acarbose, our computational model for human GAA predicted that the top binding modes of RSV localized distal to the catalytic residues in the active site pocket of GAA, thereby supporting a non-competitive mechanism *via* occupancy of GAA allosteric sites. Moreover, *in silico* modeling predicted the ability of RSV to operate as a kifunensine-like molecule capable of competitively occupying the catalytic site of the α-Man I enzyme, altogether offering an unforeseen mechanistic scenario

linking the early recognized capacity of *N*-linked glycosylation to influence lifespan with the ability of RSV to directly block GAA and α-Man and activate an ER stress (dietary restriction-like) response [108, 55, 56]. Therefore, from an immunomodulatory perspective, our present findings propose that RSV might unexpectedly operate as a member of the upstream-type of CRMs, which employ a mechanism of action involving direct targeting of glucose metabolism (i.e., inhibition of class I glycosydases) and transmit a signal in the upstream direction to mimic CR.

Cancer immunomodulation involves the use of synthetic or natural agents capable of activating the immune response to impede tumor cell dissemination. The nutraceutical RSV, a natural polyphenolic phytoalexin that is present in red wine, red grape skin, berries, peanuts, and other natural sources, has recently been proposed as a cancer immunomodulatory molecule by either acting on immune cells or by sensitizing tumor cells to the cytotoxic effects of immune cells [109]. Our impedance-based real-time cell analysis showing that cytotoxic T-lymphocyte activity is dramatically exacerbated when highly aggressive cancer cells overexpressing PD-L1 in almost 100% of the cells were previously exposed to RSV strongly suggests that, beyond promoting abnormal PD-L1 glycosylation, RSV might be targeting the immunosuppressive signaling of PD-L1 by additional mechanisms. Computer-aided docking/MD simulations predicted the ability of RSV to locate at the center of the PD-L1 homodimer, filling a deep hydrophobic pocket that contributes multiple additional interactions between the PD-L1 monomers. Indeed, RSV was predicted to almost perfectly occupy the target space of Bristol-Myers Squibb (BMS)-developed nonpeptidic chemical inhibitors such as BMS-8, BMS-202, or BMS-1166, which have a common scaffold and interact with the cavity formed by two PD-L1 monomers, (consisting of Ile54, Tyr56, Met115, Ile116, Ala121, and Tyr123 [71, 77]), thereby blocking the PD-1/PD-L1 interaction by inducing PD-L1dimerization. The double-strike PD-1/PD-L1 immune checkpoint inhibitor-like behavior of RSV based on its ability to directly target PD-L1 either *via* key post-translational modifications such as *N*-linked glycosylation [110–114] or *via* direct binding to PD-L1 to block PD-1 binding [71–77] interferes with PD-L1 stability and trafficking, impedes the correct targeting of PD-L1 to the cancer cell plasma membrane, and lastly elicits considerably enhanced cytotoxic T-lymphocyte immune-surveillance against tumor cells (Figure 9). This unforeseen immunomodulating mechanism of RSV might provide new approaches to restore T-cell function by targeting the PD-1/PD-L1 immunologic checkpoint with natural polyphenols.

MATERIALS AND METHODS

Cell lines and culture conditions

JIMT-1 cells were obtained from the German Collection of Microorganisms and Cell Culture (Braunschweig, Germany) and grown in Dulbecco's modified Eagle's medium (DMEM) supplemented with 10% heat-inactivated fetal bovine serum (FBS; BioWhittaker Inc., Walkersville, MD), 1% L-glutamine, 1% sodium pyruvate, 50 U/mL penicillin, and 50 µg/mL strep-tomycin. MDA-MB-231 breast cancer cells were obtained from the American Type Culture Collection (Manassas, VA) and grown in Improved MEM (IMEM; BioSource International, Camarillo, CA) supplemented as above. All cells were maintained at 37°C in a humidified atmosphere of 95% air and 5% CO_2. Cells were screened periodically for *Mycoplasma* contamination.

Approximately 250,000 cells were seeded in 60-mm dishes and treated with 100 µmol/L RSV (R5010), 5 mmol/L metformin (D150959), 100 µmol/L phenformin (P7045) (all from Sigma-Aldrich, St Louis, MO), 100 nmol/L soraphen A (kindly provided by Drs. Klaus Gerth and Rolf Jansen, Hemholtz Zentrum für Infektionsforschung GmbH, Braunschweig, Germany), 5 µg/mL C75 (C5490; Sigma-Aldrich), 200 nmol/L PP242 (S2218; Selleckchem, Houston, TX), 200 nmol/L Torin 2 (S2817; Selleckchem), 500 µmol/L AICAR (Cat. # sc-200659; Santa Cruz Biotechnology, Santa Cruz, CA), 5 µmol/L compound C (S7840, Selleckchem), 5 µg/mL tunicamycin (sc-3506, Santa Cruz Biotechnology), 20 µmol/L cycloheximide (sc-3508, Santa Cruz Biotechnology), 1 µmol/L MG-132 (S2619, Selleckchem), 10 µmol/L chloroquine (C6628, Sigma-Aldrich), 10 µmol/L EX-527 (S1541, Selleckchem), 10–50 µmol/L AR-A014418 (S7435, Selleckchem), or 20 mmol/L LiCl (L5509, Sigma-Aldrich) as single agents or in combination, as specified. In parallel, the untreated cultures were used as controls.

Western blotting

Following treatment with the above-mentioned drugs, cells were lysed in 2% SDS, 1% glycerol, and 5 mmol/L Tris-HCl, pH 6.8. Samples were sonicated for 1 min (under ice water bath conditions) with 2 s sonication and 2 s intervals to fully lyse cells and reduce viscosity. Alternatively, cell samples were extracted with lysis buffer (150 mmol/L NaCl, 50 mmol/L Tris-HCl pH 7.4, 1 mmol/L EDTA, 1% Triton-X 100, 1 mmol/L phenylmethylsulfonyl fluoride, 1 mmol/L Na_3VO_4) and then incubated in the presence or absence of either PNGase F (P0704S, 1,000 Units/reaction) or Endo H (P0702S, 2,000 Units/reaction) (both from New England Biolabs, Ipswich, MA) for 2 h at 37°C using 30 µg of total protein per reaction. Protein content was determined by the Bradford protein assay (Bio-Rad, Hercules, CA). Sample buffer was added to extracts and boiled for 4 min at 100°C. Equal amounts of cellular protein were electrophoresed on 12% SDS-PAGE gels, transferred to nitrocellulose membranes, and incubated with antibodies against PD-L1 (E1L3N® XP® Rabbit mAb #13684), SIRT1 (C14H14 Rabbit mAb #2496), or acetyl-p53 (Lys382) (antibody #2525) (all from Cell Signaling Technology, Danvers, MA), followed by incubation with a horseradish peroxidase-conjugated secondary antibody, and chemiluminescence detection. Vinculin (sc-25336; Santa Cruz Biotechnology; 1:10,000 dilution) and β-actin (Cat. # 66009-1-Ig, Clone #: 2D4H5; Proteintech Group, Inc., Rosemont, IL) were employed as controls for protein loading.

Immunofluorescence

Cells were seeded onto glass coverslips, treated with RSV for 24 h and then fixed with 4% paraformaldehyde in phosphate buffered saline (PBS). Following fixation at room temperature (RT) for 5 min, cells were permeabilized with 0.1% Triton X100/PBS. The coverslips were then placed in the antibody solution (E1L3N® XP® Rabbit mAb #13684 1:1,00 dilution or PD-L1 extracellular domain specific E1J2J rabbit mAb #15165 1:1,00 dilution, both from Cell Signaling Technology) and incubated for 60 min at RT. Cells were washed and stained with a secondary antibody. Cell nuclei were counterstained with Hoechst 33342. Images were captured using an Eclipse 50i fluorescence microscope equipped with NIS-Elements imaging software (Nikon, Tokyo, Japan).

Molecular docking

Acidic human α-glucosidase (UniProt code: Q16706, PDB code: 5NN4), human ER α-mannosidase I (UniProt code: Q9UKMT, PDB code: 5KIJ), *Saccharomyces cerevisiae* α-glucosidase (UniProt code: P53008, PDB code: 4J5T), and PD-L1 (UniProt code: Q9NZQ7, PDB code: 5J89) crystallographic structures were obtained from the Research Collaboratory for Structural Bioinformatics (RCSB) Protein Data Bank (PDB). In the case of the human α-mannosidase II (UniProt code: Q16706), which lacks a high-resolution available PDB structure, a homology model was generated employing the 1QWU structure (a 1.2-Å resolution structure for the Golgi α-Man II from *Drosophila melanogaster*) as a template. The specific edition of protein structures was made using PyMol software (PyMOL Molecular Graphics System, v2.3.3 Schrödinger, LLC, at http://www.pymol.org/) without further optimization.

Molecular docking experiments were carried out using YASARA v19.9.17 software executing the AutoDock 4 algorithm with AMBER99 as a force field [115–118]. Briefly, a total of 999 flexible docking runs were set and clustered (7 Å) around the putative binding sites, that is, two complexed compounds belong to different clusters if the ligand Root-Mean-Square Deviation of their atomic positions is greater than a minimum of 7 Å around certain hot spot conformations. The YASARA pH command was set to 5.0, 7.2, 7.2, and 6.4 when running the molecular docking simulations of acidic human α-glucosidase, human ER α-mannosidase I, *S. cerevisiae* α-glucosidase, and human Golgi α-mannosidase II homology model, respectively. The YASARA software calculated the Gibbs free energy variation (ΔG, kcal/mol), with more positive energy values indicating stronger binding. To calculate this parameter, Autodock Vina uses a force field scoring function that considers the strength of electrostatic interactions, hydrogen bonding between all atoms of the two binding partners in the complex, intermolecular van der Waals forces, and also solvation and entropy contributions [119]. All the values are included in the corresponding tables with a negative sign. Only the ΔG value for the best RSV docked in each cluster is shown. Dissociation constants were recalculated from the average binding energy of all RSVs of each cluster. The number of RSV docked molecules in each cluster was identified as "members" (in percentages).

Molecular dynamics simulations

YASARA dynamics v19.9.17 was used for all the MD simulations with AMBER14 as a force field. The simulation cell was allowed to include 20 Å surrounding the protein and filled with water at a density of 0.997 g/mL. Initial energy minimization was carried out under relaxed constraints using steepest descent minimization. Simulations were performed in water at constant pressure-constant temperature (25°C) conditions. To mimic physiological conditions, counter ions were added to neutralize the system; Na^+ or Cl^- were added in replacement of water to give a total NaCl concentration of 0.9% and pH was maintained at 7.4. Hydrogen atoms were added to the protein structure at the appropriate ionizable groups according to the calculated pKa in relation to the simulation pH (i.e., a hydrogen atom will be added if the computed pKa is higher than the pH). The pKa was computed for each residue according to the Ewald method [120]. All simulation steps were run by a preinstalled macro (md_run.mcr) within the YASARA suite. Data were collected every 10 ps. The molecular mechanics/

Poisson-Boltzmann surface area (MM/PBSA) was implemented with the YASARA macro md_analyzebindenergy.mcr to calculate the binding free energy with solvation of the ligand, complex, and free protein, as previously described [121–123].

All of the figures were prepared using PyMol 2.0 software and all interactions were detected using the PLIP algorithm [124].

Human T-cell culture

To acquire activated T-cells, human peripheral blood mononuclear cells (Cat. #70025) were cultured in ImmunoCult-XF™ T cell expansion medium (Cat. #10981) containing ImmunoCult-XF™ Human CD3/CD28/CD2 T-cell activator (Cat. #10971) (all from StemCell Technologies, Vancouver, BC, Canada), and 10 ng/mL IL-2 (Cat. #200-02; PeproTech, Rocky Hill, NJ) for one week, as per the manufacturers' instructions.

Cytolytic T-cell assay

T-cell-mediated lysis of tumor cells was monitored using an impedance-based approach. One hundred microliters of DMEM containing 10% FBS was added to each well of an E-Plate 16 (Roche Applied Sciences, Indianapolis, IN). Background impedance was measured using the xCELLigence RTCA instrument (Roche) at 37°C and 5% CO_2. Tumor cells were harvested, counted, and resuspended at a density of 5×10^4 cells/mL in DMEM with 10% FBS, and 100 µL of the tumor cell suspension was added to each well of the E-Plate 16. Impedance was measured every 5 minutes for approximately 24 h, as described. Media from E-Plate 16 wells were removed and replaced with unsupplemented culture media in control wells or media containing 100 µg/mL RSV in experimental wells, and impedance was measured every 5 minutes for approximately 24 h. T-cells were counted and resuspended at a concentration of 5×10^5 cells/mL in DMEM including an antii-CD3 antibody (Cat. #16-0037, 100 ng/mL; eBioscience, Thermo Fisher Scientific Inc., Philadelphia, PA). One hundred microliters of the T-cell suspension or media alone was added to respective wells and impedance was measured every 5 minutes for an additional 24 h. T-cell-mediated cell death of tumor cells was monitored in real-time and indicated as a decrease in the so-called cell index (CI) obtained using RTCA Software 1.2 (Acea Biosciences, San Diego, CA). Results were normalized to 1 to 2 h following T-cell addition. Cytolytic activity was calculated as the percentage of cytolysis 5 and 10 hours after the normalization time $(=[CI_{no\ effector}-CI_{effector}]/CI_{no\ effector} \times 100)$.

Statistical analysis

Cytolytic activity means were compared using a two-way ANOVA with Sidak's multiple comparison post-test. Results were designated significant when the P-value was < 0.01.

CONFLICTS OF INTEREST

The authors declare no conflicts of interest.

REFERENCES

1. Dieci MV, Griguolo G, Miglietta F, Guarneri V. The immune system and hormone-receptor positive breast cancer: is it really a dead end? Cancer Treat Rev. 2016; 46:9–19.
   https://doi.org/10.1016/j.ctrv.2016.03.011
   PMID:27055087

2. Solinas C, Gombos A, Latifyan S, Piccart-Gebhart M, Kok M, Buisseret L. Targeting immune checkpoints in breast cancer: an update of early results. ESMO Open. 2017; 2:e000255.
   https://doi.org/10.1136/esmoopen-2017-000255
   PMID:29177095

3. Vonderheide RH, Domchek SM, Clark AS. Immunotherapy for Breast Cancer: What Are We Missing? Clin Cancer Res. 2017; 23:2640–46.
   https://doi.org/10.1158/1078-0432.CCR-16-2569
   PMID:28572258

4. Santa-Maria CA, Nanda R. Immune Checkpoint Inhibitor Therapy in Breast Cancer. J Natl Compr Canc Netw. 2018; 16:1259–68.
   https://doi.org/10.6004/jnccn.2018.7046
   PMID:30323094

5. Chrétien S, Zerdes I, Bergh J, Matikas A, Foukakis T. Beyond PD-1/PD-L1 Inhibition: What the Future Holds for Breast Cancer Immunotherapy. Cancers (Basel). 2019; 11:E628.
   https://doi.org/10.3390/cancers11050628
   PMID:31060337

6. Ali HR, Provenzano E, Dawson SJ, Blows FM, Liu B, Shah M, Earl HM, Poole CJ, Hiller L, Dunn JA, Bowden SJ, Twelves C, Bartlett JM, et al. Association between CD8+ T-cell infiltration and breast cancer survival in 12,439 patients. Ann Oncol. 2014; 25:1536–43.
   https://doi.org/10.1093/annonc/mdu191
   PMID:24915873

7. Ali HR, Glont SE, Blows FM, Provenzano E, Dawson SJ, Liu B, Hiller L, Dunn J, Poole CJ, Bowden S, Earl HM, Pharoah PD, Caldas C. PD-L1 protein expression in breast cancer is rare, enriched in basal-like tumours and associated with infiltrating lymphocytes. Ann Oncol. 2015; 26:1488–93.
   https://doi.org/10.1093/annonc/mdv192
   PMID:25897014

8. Buisseret L, Garaud S, de Wind A, Van den Eynden G, Boisson A, Solinas C, Gu-Trantien C, Naveaux C, Lodewyckx JN, Duvillier H, Craciun L, Veys I, Larsimont D, et al. Tumor-infiltrating lymphocyte composition, organization and PD-1/ PD-L1 expression are linked in breast cancer. Oncoimmunology. 2016; 6:e1257452.
   https://doi.org/10.1080/2162402X.2016.1257452
   PMID:28197375

9. Katz H, Alsharedi M. Immunotherapy in triple-negative breast cancer. Med Oncol. 2017; 35:13.
   https://doi.org/10.1007/s12032-017-1071-6
   PMID:29255938

10. Solinas C, Garaud S, De Silva P, Boisson A, Van den Eynden G, de Wind A, Risso P, Rodrigues Vitória J, Richard F, Migliori E, Noël G, Duvillier H, Craciun L, et al. Immune Checkpoint Molecules on Tumor-Infiltrating Lymphocytes and Their Association with Tertiary Lymphoid Structures in Human Breast Cancer. Front Immunol. 2017; 8:1412.
    https://doi.org/10.3389/fimmu.2017.01412
    PMID:29163490

11. Jia H, Truica CI, Wang B, Wang Y, Ren X, Harvey HA, Song J, Yang JM. Immunotherapy for triple-negative breast cancer: existing challenges and exciting

prospects. Drug Resist Updat. 2017; 32:1–15.
https://doi.org/10.1016/j.drup.2017.07.002
PMID:29145974

12. Li Z, Qiu Y, Lu W, Jiang Y, Wang J. Immunotherapeutic interventions of Triple Negative Breast Cancer. J Transl Med. 2018; 16:147.
https://doi.org/10.1186/s12967-018-1514-7
PMID:29848327

13. Monypenny J, Milewicz H, Flores-Borja F, Weitsman G, Cheung A, Chowdhury R, Burgoyne T, Arulappu A, Lawler K, Barber PR, Vicencio JM, Keppler M, Wulaningsih W, et al. ALIX Regulates Tumor-Mediated Immunosuppression by Controlling EGFR Activity and PD-L1 Presentation. Cell Rep. 2018; 24:630–41.
https://doi.org/10.1016/j.celrep.2018.06.066
PMID:30021161

14. Vikas P, Borcherding N, Zhang W. The clinical promise of immunotherapy in triple-negative breast cancer. Cancer Manag Res. 2018; 10:6823–33.
https://doi.org/10.2147/CMAR.S185176
PMID:30573992

15. Kim A, Lee SJ, Kim YK, Park WY, Park DY, Kim JY, Lee CH, Gong G, Huh GY, Choi KU. Programmed death-ligand 1 (PD-L1) expression in tumour cell and tumour infiltrating lymphocytes of HER2-positive breast cancer and its prognostic value. Sci Rep. 2017; 7:11671.
https://doi.org/10.1038/s41598-017-11905-7
PMID:28916815

16. Li Y, Opyrchal M, Yao S, Peng X, Yan L, Jabbour H, Khoury T. The role of programmed death ligand-1 and tumor-infiltrating lymphocytes in breast cancer overexpressing HER2 gene. Breast Cancer Res Treat. 2018; 170:293–302.
https://doi.org/10.1007/s10549-018-4745-7
PMID:29524062

17. Holgado E, Perez-Garcia J, Gion M, Cortes J. Is there a role for immunotherapy in HER2-positive breast cancer? NPJ Breast Cancer. 2018; 4:21.
https://doi.org/10.1038/s41523-018-0072-8
PMID:30131972

18. Wang X, Qi Y, Kong X, Zhai J, Li Y, Song Y, Wang J, Feng X, Fang Y. Immunological therapy: A novel thriving area for triple-negative breast cancer treatment. Cancer Lett. 2019; 442:409–28.
https://doi.org/10.1016/j.canlet.2018.10.042
PMID:30419345

19. Ayoub NM, Al-Shami KM, Yaghan RJ. Immunotherapy for HER2-positive breast cancer: recent advances and combination therapeutic approaches. Breast Cancer (Dove Med Press). 2019; 11:53–69.

https://doi.org/10.2147/BCTT.S175360
PMID:30697064

20. Griguolo G, Pascual T, Dieci MV, Guarneri V, Prat A. Interaction of host immunity with HER2-targeted treatment and tumor heterogeneity in HER2-positive breast cancer. J Immunother Cancer. 2019; 7:90.
https://doi.org/10.1186/s40425-019-0548-6
PMID:30922362

21. Pardoll DM. The blockade of immune checkpoints in cancer immunotherapy. Nat Rev Cancer. 2012; 12:252–64.
https://doi.org/10.1038/nrc3239
PMID:22437870

22. Zou W, Chen L. Inhibitory B7-family molecules in the tumour microenvironment. Nat Rev Immunol. 2008; 8:467–77.
https://doi.org/10.1038/nri2326
PMID:18500231

23. Yao S, Zhu Y, Chen L. Advances in targeting cell surface signalling molecules for immune modulation. Nat Rev Drug Discov. 2013; 12:130–46.
https://doi.org/10.1038/nrd3877
PMID:23370250

24. Nanda R, Chow LQ, Dees EC, Berger R, Gupta S, Geva R, Pusztai L, Pathiraja K, Aktan G, Cheng JD, Karantza V, Buisseret L. Pembrolizumab in Patients With Advanced Triple-Negative Breast Cancer: Phase Ib KEYNOTE-012 Study. J Clin Oncol. 2016; 34:2460–67.
https://doi.org/10.1200/JCO.2015.64.8931
PMID:27138582

25. Schmid P, Adams S, Rugo HS, Schneeweiss A, Barrios CH, Iwata H, Diéras V, Hegg R, Im SA, Shaw Wright G, Henschel V, Molinero L, Chui SY, et al, and IMpassion130 Trial Investigators. Atezolizumab and Nab-Paclitaxel in Advanced Triple-Negative Breast Cancer. N Engl J Med. 2018; 379:2108–21.
https://doi.org/10.1056/NEJMoa1809615
PMID:30345906

26. Adams S, Loi S, Toppmeyer D, Cescon DW, De Laurentiis M, Nanda R, Winer EP, Mukai H, Tamura K, Armstrong A, Liu MC, Iwata H, Ryvo L, et al. Pembrolizumab monotherapy for previously untreated, PD-L1-positive, metastatic triple-negative breast cancer: cohort B of the phase II KEYNOTE-086 study. Ann Oncol. 2019; 30:405–11.
https://doi.org/10.1093/annonc/mdy518
PMID:30475947

27. Adams S, Schmid P, Rugo HS, Winer EP, Loirat D, Awada A, Cescon DW, Iwata H, Campone M, Nanda R, Hui R, Curigliano G, Toppmeyer D, et al. Pembrolizumab monotherapy for previously treated metastatic triple-negative breast cancer: cohort A of

the phase II KEYNOTE-086 study. Ann Oncol. 2019; 30:397–404.
https://doi.org/10.1093/annonc/mdy517
PMID:30475950

28. Dirix LY, Takacs I, Jerusalem G, Nikolinakos P, Arkenau HT, Forero-Torres A, Boccia R, Lippman ME, Somer R, Smakal M, Emens LA, Hrinczenko B, Edenfield W, et al. Avelumab, an anti-PD-L1 antibody, in patients with locally advanced or metastatic breast cancer: a phase 1b JAVELIN Solid Tumor study. Breast Cancer Res Treat. 2018; 167:671–86.
https://doi.org/10.1007/s10549-017-4537-5
PMID:29063313

29. Schmid P, Cruz C, Braiteh FS, Eder JP, Tolaney S, Kuter I, Nanda R, Chung C, Cassier P, Delord JP, Gordon M, Li Y, Liu B, et al. Abstract 2986: atezolizumab in metastatic TNBC (mTNBC): Long-term clinical outcomes and biomarker analyses. Cancer Res. 2017; 77:2986.
https://doi.org/10.1158/1538-7445.am2017-2986

30. Ho PC, Liu PS. Metabolic communication in tumors: a new layer of immunoregulation for immune evasion. J Immunother Cancer. 2016; 4:4.
https://doi.org/10.1186/s40425-016-0109-1
PMID:26885366

31. Allison KE, Coomber BL, Bridle BW. Metabolic reprogramming in the tumour microenvironment: a hallmark shared by cancer cells and T lymphocytes. Immunology. 2017; 152:175–84.
https://doi.org/10.1111/imm.12777
PMID:28621843

32. Sugiura A, Rathmell JC. Metabolic Barriers to T Cell Function in Tumors. J Immunol. 2018; 200:400–07.
https://doi.org/10.4049/jimmunol.1701041
PMID:29311381

33. Singer K, Cheng WC, Kreutz M, Ho PC, Siska PJ. Immunometabolism in cancer at a glance. Dis Model Mech. 2018; 11:dmm034272.
https://doi.org/10.1242/dmm.034272
PMID:30076128

34. Li X, Wenes M, Romero P, Huang SC, Fendt SM, Ho PC. Navigating metabolic pathways to enhance antitumour immunity and immunotherapy. Nat Rev Clin Oncol. 2019; 16:425–41.
https://doi.org/10.1038/s41571-019-0203-7
PMID:30914826

35. Renner K, Singer K, Koehl GE, Geissler EK, Peter K, Siska PJ, Kreutz M. Metabolic Hallmarks of Tumor and Immune Cells in the Tumor Microenvironment. Front Immunol. 2017; 8:248.
https://doi.org/10.3389/fimmu.2017.00248
PMID:28337200

36. Ramapriyan R, Caetano MS, Barsoumian HB, Mafra AC, Zambalde EP, Menon H, Tsouko E, Welsh JW, Cortez MA. Altered cancer metabolism in mechanisms of immunotherapy resistance. Pharmacol Ther. 2019; 195:162–71.
https://doi.org/10.1016/j.pharmthera.2018.11.004
PMID:30439456

37. Kouidhi S, Ben Ayed F, Benammar Elgaaied A. Targeting Tumor Metabolism: A New Challenge to Improve Immunotherapy. Front Immunol. 2018; 9:353.
https://doi.org/10.3389/fimmu.2018.00353
PMID:29527212

38. Guo C, Chen S, Liu W, Ma Y, Li J, Fisher PB, Fang X, Wang XY. Immunometabolism: A new target for improving cancer immunotherapy. Adv Cancer Res. 2019; 143:195–253.
https://doi.org/10.1016/bs.acr.2019.03.004
PMID:31202359

39. Verdura S, Cuyàs E, Martin-Castillo B, Menendez JA. Metformin as an archetype immuno-metabolic adjuvant for cancer immunotherapy. Oncoimmunology. 2019; 8:e1633235.
https://doi.org/10.1080/2162402X.2019.1633235
PMID:31646077

40. Rom-Jurek EM, Kirchhammer N, Ugocsai P, Ortmann O, Wege AK, Brockhoff G. Regulation of Programmed Death Ligand 1 (PD-L1) Expression in Breast Cancer Cell Lines In Vitro and in Immunodeficient and Humanized Tumor Mice. Int J Mol Sci. 2018; 19:E563.
https://doi.org/10.3390/ijms19020563
PMID:29438316

41. Li CW, Lim SO, Xia W, Lee HH, Chan LC, Kuo CW, Khoo KH, Chang SS, Cha JH, Kim T, Hsu JL, Wu Y, Hsu JM, et al. Glycosylation and stabilization of programmed death ligand-1 suppresses T-cell activity. Nat Commun. 2016; 7:12632.
https://doi.org/10.1038/ncomms12632
PMID:27572267

42. Chao SC, Chen YJ, Huang KH, Kuo KL, Yang TH, Huang KY, Wang CC, Tang CH, Yang RS, Liu SH. Induction of sirtuin-1 signaling by resveratrol induces human chondrosarcoma cell apoptosis and exhibits antitumor activity. Sci Rep. 2017; 7:3180.
https://doi.org/10.1038/s41598-017-03635-7
PMID:28600541

43. Lee JH, Kim JS, Park SY, Lee YJ. Resveratrol induces human keratinocyte damage via the activation of class III histone deacetylase, Sirt1. Oncol Rep. 2016; 35:524–29.
https://doi.org/10.3892/or.2015.4332
PMID:26499368

44. Chai R, Fu H, Zheng Z, Liu T, Ji S, Li G. Resveratrol inhibits proliferation and migration through SIRT1 mediated post-translational modification of PI3K/AKT signaling in hepatocellular carcinoma cells. Mol Med Rep. 2017; 16:8037–44.
https://doi.org/10.3892/mmr.2017.7612
PMID:28983625

45. Venturelli S, Berger A, Böcker A, Busch C, Weiland T, Noor S, Leischner C, Schleicher S, Mayer M, Weiss TS, Bischoff SC, Lauer UM, Bitzer M. Resveratrol as a pan-HDAC inhibitor alters the acetylation status of histone [corrected] proteins in human-derived hepatoblastoma cells. PLoS One. 2013; 8:e73097.
https://doi.org/10.1371/journal.pone.0073097
PMID:24023672

46. Bassett SA, Barnett MP. The role of dietary histone deacetylases (HDACs) inhibitors in health and disease. Nutrients. 2014; 6:4273–301.
https://doi.org/10.3390/nu6104273 PMID:25322459

47. Kai L, Samuel SK, Levenson AS. Resveratrol enhances p53 acetylation and apoptosis in prostate cancer by inhibiting MTA1/NuRD complex. Int J Cancer. 2010; 126:1538–48.
https://doi.org/10.1002/ijc.24928 PMID:19810103

48. Solomon JM, Pasupuleti R, Xu L, McDonagh T, Curtis R, DiStefano PS, Huber LJ. Inhibition of SIRT1 catalytic activity increases p53 acetylation but does not alter cell survival following DNA damage. Mol Cell Biol. 2006; 26:28–38.
https://doi.org/10.1128/MCB.26.1.28-38.2006
PMID:16354677

49. Gwak H, Kim S, Dhanasekaran DN, Song YS. Resveratrol triggers ER stress-mediated apoptosis by disrupting N-linked glycosylation of proteins in ovarian cancer cells. Cancer Lett. 2016; 371:347–53.
https://doi.org/10.1016/j.canlet.2015.11.032
PMID:26704305

50. Li CW, Lim SO, Chung EM, Kim YS, Park AH, Yao J, Cha JH, Xia W, Chan LC, Kim T, Chang SS, Lee HH, Chou CK, et al. Eradication of Triple-Negative Breast Cancer Cells by Targeting Glycosylated PD-L1. Cancer Cell. 2018; 33:187–201.e10.
https://doi.org/10.1016/j.ccell.2018.01.009
PMID:29438695

51. Zhang AJ, Rimando AM, Mizuno CS, Mathews ST. α-Glucosidase inhibitory effect of resveratrol and piceatannol. J Nutr Biochem. 2017; 47:86–93.
https://doi.org/10.1016/j.jnutbio.2017.05.008
PMID:28570943

52. Kerem Z, Bilkis I, Flaishman MA, Sivan L. Antioxidant activity and inhibition of alpha-glucosidase by trans-resveratrol, piceid, and a novel trans-stilbene from the roots of Israeli Rumex bucephalophorus L. J Agric Food Chem. 2006; 54:1243–47.
https://doi.org/10.1021/jf052436+
PMID:16478243

53. Carpéné C, Les F, Cásedas G, Peiro C, Fontaine J, Chaplin A, Mercader J, López V. Resveratrol Anti-Obesity Effects: Rapid Inhibition of Adipocyte Glucose Utilization. Antioxidants. 2019; 8:E74.
https://doi.org/10.3390/antiox8030074
PMID:30917543

54. Shen Y, Xu Z, Sheng Z. Ability of resveratrol to inhibit advanced glycation end product formation and carbohydrate-hydrolyzing enzyme activity, and to conjugate methylglyoxal. Food Chem. 2017; 216:153–60.
https://doi.org/10.1016/j.foodchem.2016.08.034
PMID:27596404

55. Viswanathan M, Kim SK, Berdichevsky A, Guarente L. A role for SIR-2.1 regulation of ER stress response genes in determining C. elegans life span. Dev Cell. 2005; 9:605–15.
https://doi.org/10.1016/j.devcel.2005.09.017
PMID:16256736

56. Liu YL, Lu WC, Brummel TJ, Yuh CH, Lin PT, Kao TY, Li FY, Liao PC, Benzer S, Wang HD. Reduced expression of alpha-1,2-mannosidase I extends lifespan in Drosophila melanogaster and Caenorhabditis elegans. Aging Cell. 2009; 8:370–79.
https://doi.org/10.1111/j.1474-9726.2009.00471.x
PMID:19302370

57. Barker MK, Rose DR. Specificity of Processing α-glucosidase I is guided by the substrate conformation: crystallographic and in silico studies. J Biol Chem. 2013; 288:13563–74.
https://doi.org/10.1074/jbc.M113.460436
PMID:23536181

58. Roig-Zamboni V, Cobucci-Ponzano B, Iacono R, Ferrara MC, Germany S, Bourne Y, Parenti G, Moracci M, Sulzenbacher G. Structure of human lysosomal acid α-glucosidase-a guide for the treatment of Pompe disease. Nat Commun. 2017; 8:1111.
https://doi.org/10.1038/s41467-017-01263-3
PMID:29061980

59. Chiasson JL, Josse RG, Gomis R, Hanefeld M, Karasik A, Laakso M, and STOP-NIDDM Trail Research Group. Acarbose for prevention of type 2 diabetes mellitus: the STOP-NIDDM randomised trial. Lancet. 2002; 359:2072–77.
https://doi.org/10.1016/S0140-6736(02)08905-5
PMID:12086760

60. Harrison DE, Strong R, Allison DB, Ames BN, Astle CM, Atamna H, Fernandez E, Flurkey K, Javors MA, Nadon

NL, Nelson JF, Pletcher S, Simpkins JW, et al. Acarbose, 17-α-estradiol, and nordihydroguaiaretic acid extend mouse lifespan preferentially in males. Aging Cell. 2014; 13:273–82.
https://doi.org/10.1111/acel.12170 PMID:24245565

61. Brewer RA, Gibbs VK, Smith DL Jr. Targeting glucose metabolism for healthy aging. Nutr Healthy Aging. 2016; 4:31–46.
https://doi.org/10.3233/NHA-160007
PMID:28035340

62. Shintani H, Shintani T, Ashida H, Sato M. Calorie Restriction Mimetics: Upstream-Type Compounds for Modulating Glucose Metabolism. Nutrients. 2018; 10:E1821.
https://doi.org/10.3390/nu10121821
PMID:30469486

63. Harrison DE, Strong R, Alavez S, Astle CM, DiGiovanni J, Fernandez E, Flurkey K, Garratt M, Gelfond JA, Javors MA, Levi M, Lithgow GJ, Macchiarini F, et al. Acarbose improves health and lifespan in aging HET3 mice. Aging Cell. 2019; 18:e12898.
https://doi.org/10.1111/acel.12898
PMID:30688027

64. Xiang Y, Karaveg K, Moremen KW. Substrate recognition and catalysis by GH47 α-mannosidases involved in Asn-linked glycan maturation in the mammalian secretory pathway. Proc Natl Acad Sci USA. 2016; 113:E7890–99.
https://doi.org/10.1073/pnas.1611213113
PMID:27856750

65. Elbein AD, Tropea JE, Mitchell M, Kaushal GP. Kifunensine, a potent inhibitor of the glycoprotein processing mannosidase I. J Biol Chem. 1990; 265:15599–605. PMID:2144287

66. Shah N, Kuntz DA, Rose DR. Comparison of kifunensine and 1-deoxymannojirimycin binding to class I and II alpha-mannosidases demonstrates different saccharide distortions in inverting and retaining catalytic mechanisms. Biochemistry. 2003; 42:13812–16.
https://doi.org/10.1021/bi034742r
PMID:14636047

67. Cha JH, Yang WH, Xia W, Wei Y, Chan LC, Lim SO, Li CW, Kim T, Chang SS, Lee HH, Hsu JL, Wang HL, Kuo CW, et al. Metformin Promotes Antitumor Immunity via Endoplasmic-Reticulum-Associated Degradation of PD-L1. Mol Cell. 2018; 71:606–620.e7.
https://doi.org/10.1016/j.molcel.2018.07.030
PMID:30118680

68. Soliman H, Khalil F, Antonia S. PD-L1 expression is increased in a subset of basal type breast cancer cells. PLoS One. 2014; 9:e88557.
https://doi.org/10.1371/journal.pone.0088557
PMID:24551119

69. Henle AM, Erskine CL, Benson LM, Clynes R, Knutson KL. Enzymatic discovery of a HER-2/neu epitope that generates cross-reactive T cells. J Immunol. 2013; 190:479–88.
https://doi.org/10.4049/jimmunol.1201264
PMID:23180824

70. Erskine CL, Henle AM, Knutson KL. Determining optimal cytotoxic activity of human Her2neu specific CD8 T cells by comparing the Cr51 release assay to the xCELLigence system. J Vis Exp. 2012; 66:e3683.
https://doi.org/10.3791/3683
PMID:22895471

71. Zak KM, Grudnik P, Guzik K, Zieba BJ, Musielak B, Dömling A, Dubin G, Holak TA. Structural basis for small molecule targeting of the programmed death ligand 1 (PD-L1). Oncotarget. 2016; 7:30323–35.
https://doi.org/10.18632/oncotarget.8730
PMID:27083005

72. Guzik K, Zak KM, Grudnik P, Magiera K, Musielak B, Törner R, Skalniak L, Dömling A, Dubin G, Holak TA. Small-Molecule Inhibitors of the Programmed Cell Death-1/Programmed Death-Ligand 1 (PD-1/PD-L1) Interaction via Transiently Induced Protein States and Dimerization of PD-L1. J Med Chem. 2017; 60:5857–67.
https://doi.org/10.1021/acs.jmedchem.7b00293
PMID:28613862

73. Zak KM, Grudnik P, Magiera K, Dömling A, Dubin G, Holak TA. Structural Biology of the Immune Checkpoint Receptor PD-1 and Its Ligands PD-L1/PD-L2. Structure. 2017; 25:1163–74.
https://doi.org/10.1016/j.str.2017.06.011
PMID:28768162

74. Konstantinidou M, Zarganes-Tzitzikas T, Magiera-Mularz K, Holak TA, Dömling A. Immune Checkpoint PD-1/PD-L1: Is There Life Beyond Antibodies? Angew Chem Int Ed Engl. 2018; 57:4840–48.
https://doi.org/10.1002/anie.201710407
PMID:29178534

75. Lim H, Chun J, Jin X, Kim J, Yoon J, No KT. Investigation of protein-protein interactions and hot spot region between PD-1 and PD-L1 by fragment molecular orbital method. Sci Rep. 2019; 9:16727.
https://doi.org/10.1038/s41598-019-53216-z
PMID:31723178

76. Guzik K, Tomala M, Muszak D, Konieczny M, Hec A, Błaszkiewicz U, Pustuła M, Butera R, Dömling A, Holak TA. Development of the Inhibitors that Target the PD-1/PD-L1 Interaction-A Brief Look at Progress on Small Molecules, Peptides and Macrocycles. Molecules.

2019; 24:E2071.
https://doi.org/10.3390/molecules24112071
PMID:31151293

77. Shi D, An X, Bai Q, Bing Z, Zhou S, Liu H, Yao X. Computational Insight Into the Small Molecule Intervening PD-L1 Dimerization and the Potential Structure-Activity Relationship. Front Chem. 2019; 7:764.
https://doi.org/10.3389/fchem.2019.00764
PMID:31781546

78. Price NL, Gomes AP, Ling AJ, Duarte FV, Martin-Montalvo A, North BJ, Agarwal B, Ye L, Ramadori G, Teodoro JS, Hubbard BP, Varela AT, Davis JG, et al. SIRT1 is required for AMPK activation and the beneficial effects of resveratrol on mitochondrial function. Cell Metab. 2012; 15:675–90.
https://doi.org/10.1016/j.cmet.2012.04.003
PMID:22560220

79. Um JH, Park SJ, Kang H, Yang S, Foretz M, McBurney MW, Kim MK, Viollet B, Chung JH. AMP-activated protein kinase-deficient mice are resistant to the metabolic effects of resveratrol. Diabetes. 2010; 59:554–63.
https://doi.org/10.2337/db09-0482
PMID:19934007

80. Lan F, Weikel KA, Cacicedo JM, Ido Y. Resveratrol-Induced AMP-Activated Protein Kinase Activation Is Cell-Type Dependent: Lessons from Basic Research for Clinical Application. Nutrients. 2017; 9:E751.
https://doi.org/10.3390/nu9070751
PMID:28708087

81. Vasconcelos-Dos-Santos A, Oliveira IA, Lucena MC, Mantuano NR, Whelan SA, Dias WB, Todeschini AR. Biosynthetic Machinery Involved in Aberrant Glycosylation: Promising Targets for Developing of Drugs Against Cancer. Front Oncol. 2015; 5:138.
https://doi.org/10.3389/fonc.2015.00138
PMID:26161361

82. O'Keefe S, Roebuck QP, Nakagome I, Hirono S, Kato A, Nash R, High S. Characterizing the selectivity of ER α-glucosidase inhibitors. Glycobiology. 2019; 29:530–42.
https://doi.org/10.1093/glycob/cwz029
PMID:30976784

83. Hsu JM, Li CW, Lai YJ, Hung MC. Posttranslational Modifications of PD-L1 and Their Applications in Cancer Therapy. Cancer Res. 2018; 78:6349–53.
https://doi.org/10.1158/0008-5472.CAN-18-1892
PMID:30442814

84. Cha JH, Chan LC, Li CW, Hsu JL, Hung MC. Mechanisms Controlling PD-L1 Expression in Cancer. Mol Cell. 2019; 76:359–70.

https://doi.org/10.1016/j.molcel.2019.09.030
PMID:31668929

85. Lee HH, Wang YN, Xia W, Chen CH, Rau KM, Ye L, Wei Y, Chou CK, Wang SC, Yan M, Tu CY, Hsia TC, Chiang SF, et al. Removal of N-Linked Glycosylation Enhances PD-L1 Detection and Predicts Anti-PD-1/PD-L1 Therapeutic Efficacy. Cancer Cell. 2019; 36:168–178.e4.
https://doi.org/10.1016/j.ccell.2019.06.008
PMID:31327656

86. Walle T. Bioavailability of resveratrol. Ann N Y Acad Sci. 2011; 1215:9–15.
https://doi.org/10.1111/j.1749-6632.2010.05842.x
PMID:21261636

87. Vang O, Ahmad N, Baile CA, Baur JA, Brown K, Csiszar A, Das DK, Delmas D, Gottfried C, Lin HY, Ma QY, Mukhopadhyay P, Nalini N, et al. What is new for an old molecule? Systematic review and recommendations on the use of resveratrol. PLoS One. 2011; 6:e19881.
https://doi.org/10.1371/journal.pone.0019881
PMID:21698226

88. Hammerl D, Smid M, Timmermans AM, Sleijfer S, Martens JW, Debets R. Breast cancer genomics and immuno-oncological markers to guide immune therapies. Semin Cancer Biol. 2018; 52:178–88.
https://doi.org/10.1016/j.semcancer.2017.11.003
PMID:29104025

89. de la Cruz-Merino L, Chiesa M, Caballero R, Rojo F, Palazón N, Carrasco FH, Sánchez-Margalet V. Breast Cancer Immunology and Immunotherapy: Current Status and Future Perspectives. Int Rev Cell Mol Biol. 2017; 331:1–53.
https://doi.org/10.1016/bs.ircmb.2016.09.008
PMID:28325210

90. de la Cruz-Merino L, Palazón-Carrión N, Henao-Carrasco F, Nogales-Fernández E, Álamo-de la Gala M, Vallejo-Benítez A, Chiesa M, Sánchez-Margalet V, and GEICAM (Spanish Breast Cancer Research Group) and GÉTICA (Spanish Group for Cancer Immuno-Biotherapy). New horizons in breast cancer: the promise of immunotherapy. Clin Transl Oncol. 2019; 21:117–25.
https://doi.org/10.1007/s12094-018-1907-3
PMID:29916188

91. Lucas J, Hsieh TC, Halicka HD, Darzynkiewicz Z, Wu JM. Upregulation of PD-L1 expression by resveratrol and piceatannol in breast and colorectal cancer cells occurs via HDAC3/p300-mediated NF-κB signaling. Int J Oncol. 2018; 53:1469–80.
https://doi.org/10.3892/ijo.2018.4512
PMID:30066852

92. Chin YT, Wei PL, Ho Y, Nana AW, Changou CA, Chen YR, Yang YS, Hsieh MT, Hercbergs A, Davis PJ, Shih YJ, Lin HY. Thyroxine inhibits resveratrol-caused apoptosis by PD-L1 in ovarian cancer cells. Endocr Relat Cancer. 2018; 25:533–45.
https://doi.org/10.1530/ERC-17-0376
PMID:29555649

93. Chen YR, Chen YS, Chin YT, Li ZL, Shih YJ, Yang YS, ChangOu CA, Su PY, Wang SH, Wu YH, Chiu HC, Lee SY, Liu LF, et al. Thyroid hormone-induced expression of inflammatory cytokines interfere with resveratrol-induced anti-proliferation of oral cancer cells. Food Chem Toxicol. 2019; 132:110693.
https://doi.org/10.1016/j.fct.2019.110693
PMID:31336132

94. Zhang Y, Yang S, Yang Y, Liu T. Resveratrol induces immunogenic cell death of human and murine ovarian carcinoma cells. Infect Agent Cancer. 2019; 14:27.
https://doi.org/10.1186/s13027-019-0247-4
PMID:31636696

95. López-Otín C, Blasco MA, Partridge L, Serrano M, Kroemer G. The hallmarks of aging. Cell. 2013; 153:1194–217.
https://doi.org/10.1016/j.cell.2013.05.039
PMID:23746838

96. Kater AP, van der Windt GJ. PD-L1 blockade: rejuvenating T cells in CLL. Blood. 2015; 126:126–28.
https://doi.org/10.1182/blood-2015-05-638338
PMID:26160184

97. Hong H, Wang Q, Li J, Liu H, Meng X, Zhang H. Aging, Cancer and Immunity. J Cancer. 2019; 10:3021–27.
https://doi.org/10.7150/jca.30723 PMID:31281479

98. Pawelec G. Does patient age influence anti-cancer immunity? Semin Immunopathol. 2019; 41:125–31.
https://doi.org/10.1007/s00281-018-0697-6
PMID:30006738

99. Ladomersky E, Scholtens DM, Kocherginsky M, Hibler EA, Bartom ET, Otto-Meyer S, Zhai L, Lauing KL, Choi J, Sosman JA, Wu JD, Zhang B, Lukas RV, Wainwright DA. The Coincidence Between Increasing Age, Immunosuppression, and the Incidence of Patients With Glioblastoma. Front Pharmacol. 2019; 10:200.
https://doi.org/10.3389/fphar.2019.00200
PMID:30971917

100. Wu Y, Wei J, Chen X, Qin Y, Mao R, Song J, Fan Y. Comprehensive transcriptome profiling in elderly cancer patients reveals aging-altered immune cells and immune checkpoints. Int J Cancer. 2019; 144:1657–63.
https://doi.org/10.1002/ijc.31875
PMID:30230534

101. Orlandella RM, Boi S, Smith D, Norian LA. Understanding the effects of a calorie restriction mimetics on renal cancer progression and CD8 T cell immunity. J Immunol 2017; 198(1 Supplement):76.12.

102. Turbitt WJ, Orlandella RM, Gibson JT, Norian LA. Acarbose, but not metformin, reduces tumor burden and improves intra-tumoral immune responses in a pre-clinical breast cancer model [abstract]. In: Proceedings of the American Association for Cancer Research Annual Meeting 2019; Atlanta, GA. Philadelphia (PA): AACR; Cancer Res 2019; 79(13 Suppl):Abstract nr 509.
https://doi.org/10.1158/1538-7445.sabcs18-509

103. Timmers S, Konings E, Bilet L, Houtkooper RH, van de Weijer T, Goossens GH, Hoeks J, van der Krieken S, Ryu D, Kersten S, Moonen-Kornips E, Hesselink MK, Kunz I, et al. Calorie restriction-like effects of 30 days of resveratrol supplementation on energy metabolism and metabolic profile in obese humans. Cell Metab. 2011; 14:612–22.
https://doi.org/10.1016/j.cmet.2011.10.002
PMID:22055504

104. Bhatt JK, Thomas S, Nanjan MJ. Resveratrol supplementation improves glycemic control in type 2 diabetes mellitus. Nutr Res. 2012; 32:537–41.
https://doi.org/10.1016/j.nutres.2012.06.003
PMID:22901562

105. Hausenblas HA, Schoulda JA, Smoliga JM. Resveratrol treatment as an adjunct to pharmacological management in type 2 diabetes mellitus—systematic review and meta-analysis. Mol Nutr Food Res. 2015; 59:147–59.
https://doi.org/10.1002/mnfr.201400173
PMID:25138371

106. Newman JC, Milman S, Hashmi SK, Austad SN, Kirkland JL, Halter JB, Barzilai N. Strategies and Challenges in Clinical Trials Targeting Human Aging. J Gerontol A Biol Sci Med Sci. 2016; 71:1424–34.
https://doi.org/10.1093/gerona/glw149
PMID:27535968

107. Oki T, Matsui T, Osajima Y. Inhibitory effect of alpha-glucosidase inhibitors varies according to its origin. J Agric Food Chem. 1999; 47:550–53.
https://doi.org/10.1021/jf980788t PMID:10563931

108. Bolanowski MA, Jacobson LA, Russell RL. Quantitative measures of aging in the nematode Caenorhabditis elegans: II. Lysosomal hydrolases as markers of senescence. Mech Ageing Dev. 1983; 21:295–319.
https://doi.org/10.1016/0047-6374(83)90048-9
PMID:6412000

109. Trung LQ, An DT. Is Resveratrol a Cancer Immunomodulatory Molecule? Front Pharmacol. 2018; 9:1255.
https://doi.org/10.3389/fphar.2018.01255
PMID:30459616

110. Wang Y, Wang H, Yao H, Li C, Fang JY, Xu J. Regulation of PD-L1: Emerging Routes for Targeting Tumor Immune Evasion. Front Pharmacol. 2018; 9:536.
https://doi.org/10.3389/fphar.2018.00536
PMID:29910728

111. Horita H, Law A, Hong S, Middleton K. Identifying Regulatory Posttranslational Modifications of PD-L1: A Focus on Monoubiquitinaton. Neoplasia. 2017; 19:346–53.
https://doi.org/10.1016/j.neo.2017.02.006
PMID:28319808

112. Yao H, Lan J, Li C, Shi H, Brosseau JP, Wang H, Lu H, Fang C, Zhang Y, Liang L, Zhou X, Wang C, Xue Y, et al. Inhibiting PD-L1 palmitoylation enhances T-cell immune responses against tumours. Nat Biomed Eng. 2019; 3:306–17.
https://doi.org/10.1038/s41551-019-0375-6
PMID:30952982

113. Wang H, Yao H, Li C, Shi H, Lan J, Li Z, Zhang Y, Liang L, Fang JY, Xu J. HIP1R targets PD-L1 to lysosomal degradation to alter T cell-mediated cytotoxicity. Nat Chem Biol. 2019; 15:42–50.
https://doi.org/10.1038/s41589-018-0161-x
PMID:30397328

114. Hsu JM, Xia W, Hsu YH, Chan LC, Yu WH, Cha JH, Chen CT, Liao HW, Kuo CW, Khoo KH, Hsu JL, Li CW, Lim SO, et al. STT3-dependent PD-L1 accumulation on cancer stem cells promotes immune evasion. Nat Commun. 2018; 9:1908.
https://doi.org/10.1038/s41467-018-04313-6
PMID:29765039

115. Krieger E, Vriend G. YASARA View - molecular graphics for all devices - from smartphones to workstations. Bioinformatics. 2014; 30:2981–82.
https://doi.org/10.1093/bioinformatics/btu426
PMID:24996895

116. Krieger E, Darden T, Nabuurs SB, Finkelstein A, Vriend G. Making optimal use of empirical energy functions: force-field parameterization in crystal space. Proteins. 2004; 57:678–83.
https://doi.org/10.1002/prot.20251
PMID:15390263

117. Morris GM, Huey R, Olson AJ. Using AutoDock for ligand-receptor docking. Curr Protoc Bioinformatics. 2008; Chapter 8:Unit 8.14.
https://doi.org/10.1002/0471250953.bi0814s24
PMID:19085980

118. Morris GM, Huey R, Lindstrom W, Sanner MF, Belew RK, Goodsell DS, Olson AJ. AutoDock4 and AutoDockTools4: automated docking with selective receptor flexibility. J Comput Chem. 2009; 30:2785–91.
https://doi.org/10.1002/jcc.21256
PMID:19399780

119. Lionta E, Spyrou G, Vassilatis DK, Cournia Z. Structure-based virtual screening for drug discovery: principles, applications and recent advances. Curr Top Med Chem. 2014; 14:1923–38.
https://doi.org/10.2174/1568026614666140929124445 PMID:25262799

120. Krieger E, Nielsen JE, Spronk CA, Vriend G. Fast empirical pKa prediction by Ewald summation. J Mol Graph Model. 2006; 25:481–86.
https://doi.org/10.1016/j.jmgm.2006.02.009
PMID:16644253

121. Cuyàs E, Verdura S, Lozano-Sánchez J, Viciano I, Llorach-Parés L, Nonell-Canals A, Bosch-Barrera J, Brunet J, Segura-Carretero A, Sanchez-Martinez M, Encinar JA, Menendez JA. The extra virgin olive oil phenolic oleacein is a dual substrate-inhibitor of catechol-O-methyltransferase. Food Chem Toxicol. 2019; 128:35–45.
https://doi.org/10.1016/j.fct.2019.03.049
PMID:30935952

122. Cuyàs E, Verdura S, Micol V, Joven J, Bosch-Barrera J, Encinar JA, Menendez JA. Revisiting silibinin as a novobiocin-like Hsp90 C-terminal inhibitor: computational modeling and experimental validation. Food Chem Toxicol. 2019; 132:110645.
https://doi.org/10.1016/j.fct.2019.110645
PMID:31254591

123. Cuyàs E, Gumuzio J, Lozano-Sánchez J, Carreras D, Verdura S, Llorach-Parés L, Sanchez-Martinez M, Selga E, Pérez GJ, Scornik FS, Brugada R, Bosch-Barrera J, Segura-Carretero A, et al. Extra Virgin Olive Oil Contains a Phenolic Inhibitor of the Histone Demethylase LSD1/KDM1A. Nutrients. 2019; 11:E1656.
https://doi.org/10.3390/nu11071656
PMID:31331073

124. Salentin S, Schreiber S, Haupt VJ, Adasme MF, Schroeder M. PLIP: fully automated protein-ligand interaction profiler. Nucleic Acids Res. 2015; 43:W443–7.
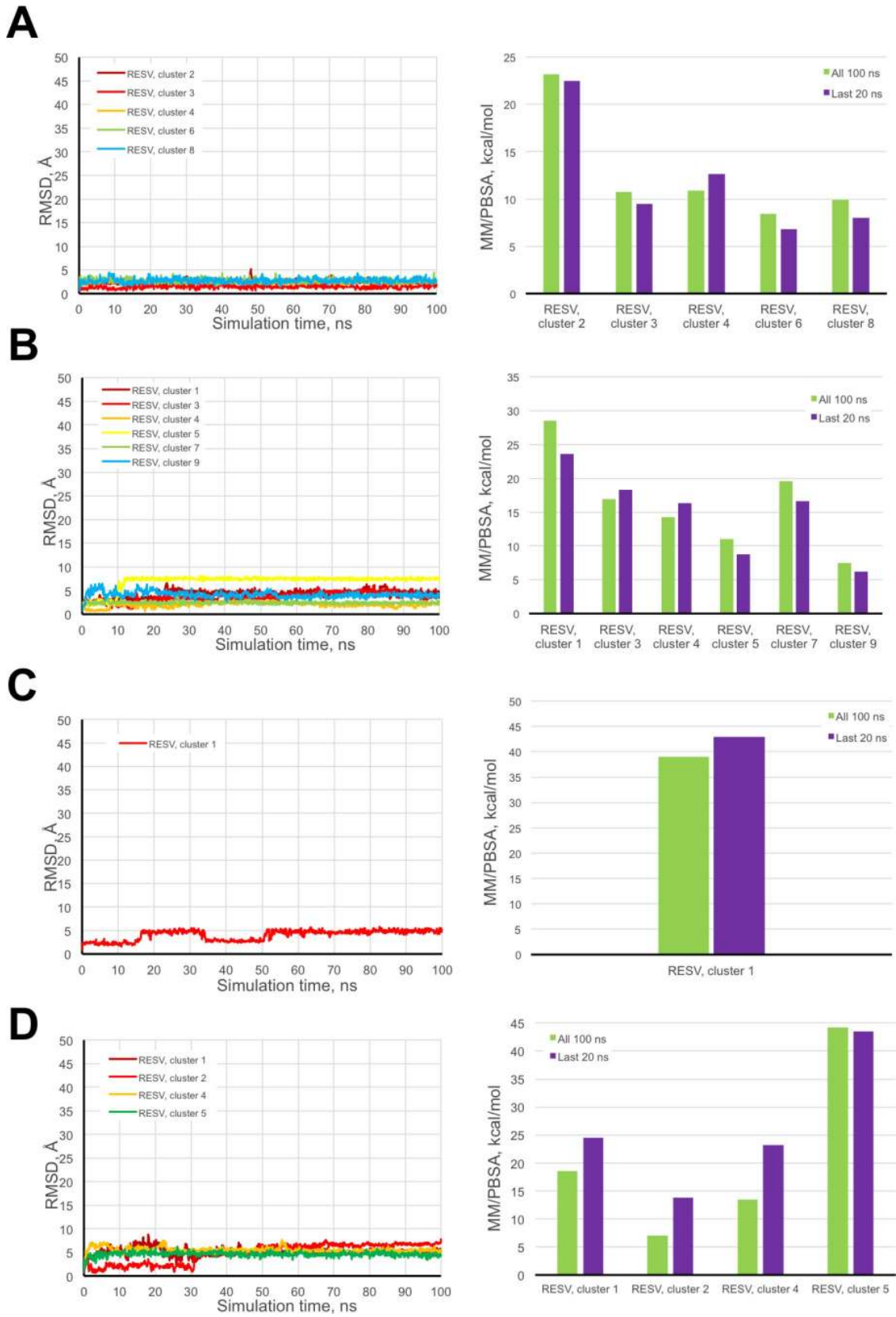https://doi.org/10.1093/nar/gkv315
PMID:25873628
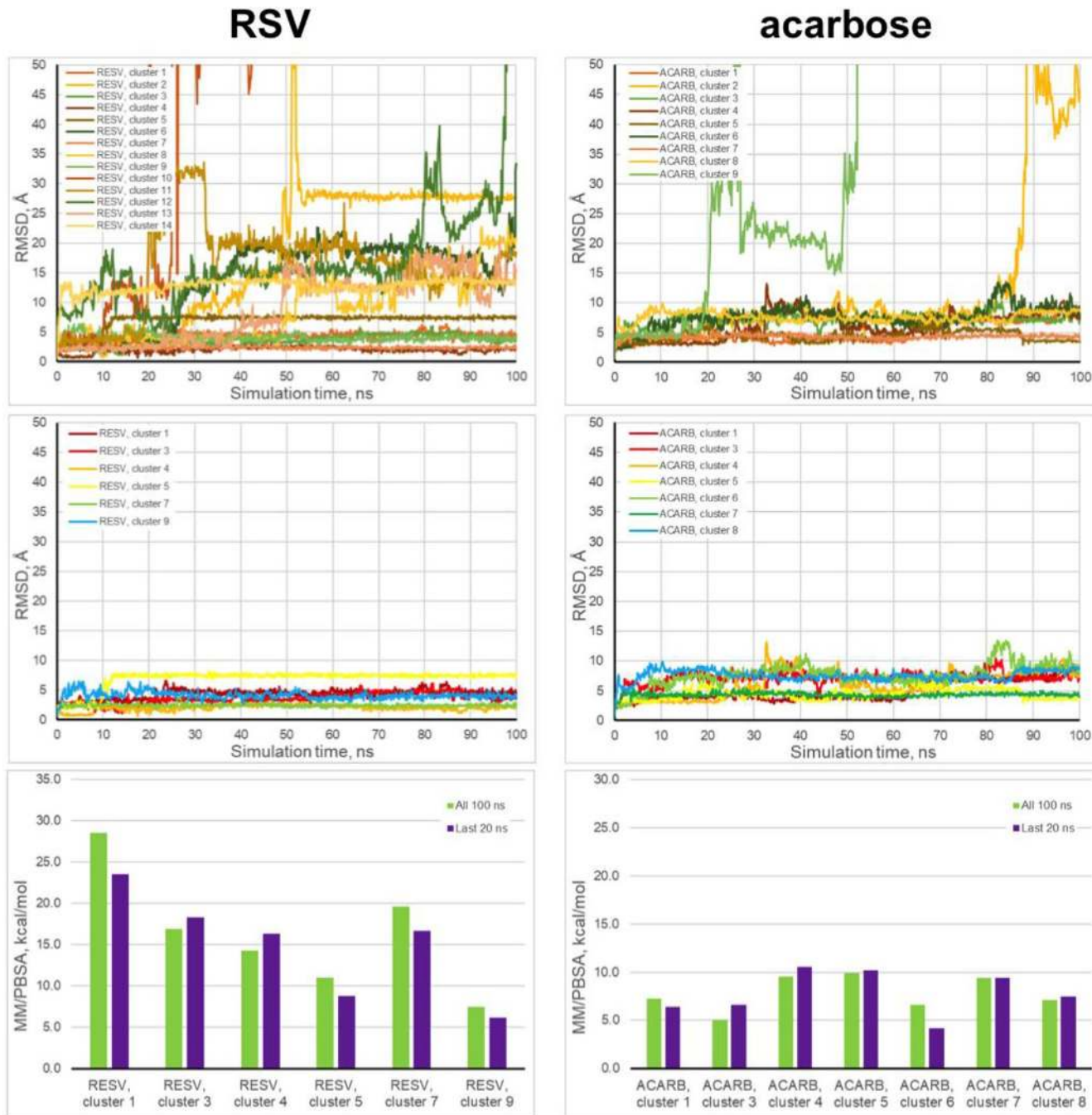
Supplementary Figure S1. Trajectories and MM/PBSA free energy analysis of RSV (*left*) and acarbose (*right*) forming complexes with the yeast form of GGA.

Supplementary Figure S2. Trajectories and MM/PBSA free energy analysis of RSV clusters forming complexes with human GAA (**A**), yeast GGA (**B**), human α-Man I (**C**), and human α-Man II homology model (**D**).

Supplementary Tables

Supplementary Table S1. Details of the interaction of RSV docked to yeast α-glucosidase.

Cluster number	ΔG, [kcal/mol]	Dissoc. constant, [µM]	Members
1	-7.89	1.650	2.9%
2	-7.43	3.590	4.1%
3	-7.28	4.640	6.9%
4	-7.08	6.420	2.6%
5	-6.78	10.770	1.8%
6	-6.76	11.160	2.3%
7	-6.66	13.160	1.9%
8	-6.64	13.540	1.4%
9	-6.55	15.870	4.1%
10	-6.53	16.310	2.9%
11	-6.43	19.360	3.8%
12	-6.33	22.950	3.8%
13	-6.30	24.190	1.3%
14	-6.27	25.250	3.2%

(Uniprot code: **P53008**, PDB code: **4J5T**). For the best-docked RSV molecule of each cluster, the Gibbs free energy (ΔG, Kcal/mol), the dissociation constant, and the number of molecules members (as %) are shown.

Supplementary Table S2. Details of the interaction of RSV docked to human α-glucosidase.

Cluster number	ΔG, [kcal/mol]	Dissoc. constant, [µM]	Members
1	-8.04	0.128	3.1%
2	-7.78	0.197	1.7%
3	-7.66	0.242	1.4%
4	-7.37	0.399	0.9%
5	-7.34	0.420	1.7%
6	-7.28	0.462	3.0%
7	-7.28	0.461	1.0%
8	-7.02	0.710	2.1%
9	-6.78	1.077	0.8%
10	-6.73	1.166	1.3%
11	-6.72	1.193	1.1%

(Uniprot code: **P10253**, PDB code: **5NN4**). For the best-docked RSV molecule of each cluster, the Gibbs free energy (ΔG, Kcal/mol), the dissociation constant, and the number of molecules members (as %) are shown.

Supplementary Table 3. **Details of the interaction of RSV docked to human α-mannosidase I.**

Cluster number	∆G, [kcal/mol]	Dissoc. constant, [µM]	Members
1	-8.25	0.892	2.1%

(Uniprot code: **Q9UKM7**, PDB code: **5KIJ**). For the best-docked RSV molecule of each cluster, the Gibbs free energy (∆G, Kcal/mol), the dissociation constant, and the number of molecules members (as %) are shown.